Doctoral Dissertation (Shinshu University)

Study on sound absorption materials/structures and their performance

（吸音材料・構造の開発とその性能評価に関する研究）

September 2023

YANG WENDAN

Abstract

The sound absorption technique is a method for noise control. In recent years, with the development of the social economy, there has been a demand for functional materials that are lighter in weight, have superior performance, and are environmentally friendly. Sound-absorbing materials are widely used as noise suppression measures in practice. However, in the design and development of sound-absorbing materials, we are still far from elucidating the mechanisms of sound insulation and sound absorption and designing optimal structures. In response to the diversification of materials and structures, the demand for functional materials, including more efficient suppression effects, recycling, and other various performances, is increasing daily. This research is to develop composite materials and structures with excellent sound absorption effects for humanly audible sounds and to establish a method for evaluating their performance. The establishment of an evaluation system for sound absorption performance of functional materials and elucidation of the mechanism was studied. In particular, we fabricated sound-absorbing materials using green composites containing waste wood and natural fibers and evaluated their performance. The obtained main results are as follows:

(1) In the first part of the work, we proposed a single cavity structure (SCRS) and a double cavity structure (DCRS) embedded with PMs and/or MPPs to enhance low-frequency absorption performance. A new sound absorption structure with two air cavities combining with a porous material or a microperforated board inside the

Helmholtz resonator was designed and fabricated. Then, the absorption coefficients and peak frequencies are systematically discussed. The findings revealed that the DCRD's sound absorption performance is more than two times higher than that of the Helmholtz resonance structure. The developed DCRD could almost absorb low-frequency sounds without sacrificing high-frequency performance by using the microperforated board of MPP 3. The optimization of absorption behavior is obtained, especially in the low-frequency region, which may offer a flexible design approach without increasing the structure's size. In addition, it is clarified that the absorption effect of SCRD with wave foam is better than that of flat foam, and the continuous round hole shape is better than slit holes.

(2) In the second part of the work, a multi-band sound-absorbing device with two air cavities was proposed, of which a double resonant structure was constructed by embedding a sound-absorbing material in the Helmholtz resonator's neck and a microperforated board inside the Helmholtz resonator, respectively. In particular, we systematically discuss the sound absorption coefficient of each assembly unit and shed light on the mechanism and structure-activity relationship of the proposed double cavity resonant device (DCRD). The results show that the sound absorption performance of the prepared DCRD is twice times higher than that of the Helmholtz resonance structure under the same content of the air cavity. Thus, it could greatly improved the absorption ratio of low-frequency sound without sacrificing high-frequency performance with the assistance of microperforated plates.

(3) In the third part of the work, the straw and rice husk are abundant and easily accessible biological resources, which are considered to be excellent candidates for

sound absorption materials for their natural porous structure. The typical sound-absorbing materials were prepared from different kinds of rice straws (thickness) and rice husks. A systematic exploration was devoted to study the effect of rice straw type and cavity thickness on the sound-absorbing performance. The results showed that rice straws with a diameter of $\geqslant$3 mm exhibited an optimized sound absorption capacity, and the performance continued to be enhanced after mixing with rice husks. In addition, the sound absorption performance of the multilayer sound absorbing structure composed of porous medium density fiberboard and thick straw and rice husk samples on the low frequency side is better than that of the multilayer sound absorbing structure using non-woven fabrics.

In summary, we believe this work provides a new toolbox for enriching the family of resonant sound absorption materials, especially realizing noise reduction optimization of low-frequency sounds through a flexible design approach without increasing the structure size.

CONTENT

Chapter 1: General introduction

1.1 Sound and noise

Noise destabilizes people's minds and bodies and interferes with their activities. Noise is known to affect the human body in addition to human hearing [1-4]. Many harmful effects have been reported, including increased fatigue, difficulty concentrating, discomfort, nausea, vomiting, decreased stomach secretions, and effects on the autonomic nervous system [5-6]. In recent years, environmental standards have been set, and people are becoming more concerned about noise, and there are still many situations in which noise control measures are necessary. The causes of the noise problem from a technological viewpoint is one way to solve these problems.

1.2 Sound reduction materials

1.2.1 Sound propagation

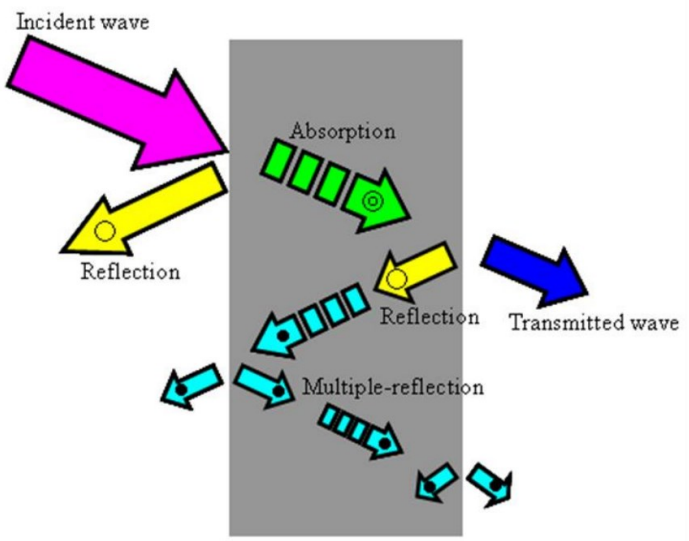

Fig.1-1 Schematic of sound propagation in materials.

When sound waves propagate in materials, there are three transformations of sound energy: reflection, absorption and transmission as imaged in Fig. 1-1 [7-10]. The total acoustic energy can be regarded as the sum of the energy reflected, absorbed and transmitted. Therefore, sound absorption is the sound energy absorbed within the material. When sound waves propagate in a closed environment, they will propagate to the surface, where some energy will be reflected. When the sound waves propagate into the material, due to the volume limitation of obstacles, the sound propagation is hindered and energy is released inside the material. In general, porous and spongy structures are generally used as absorbents. There are tiny interconnected spaces through which sound can be transmitted. As a result, sound waves lose energy due to friction between air particles and the void wall. In addition, there is energy transfer due to internal reflection or multi-reflection. For large interactions, pressure waves need to penetrate into the material so that it does not reflect. If the size of the hole is large, the energy transferred in the material increases, so more energy is absorbed by the material. Similarly, if the size of the hole is very small, the energy transferred to the solid structure will be reduced, so more energy will be reflected from the surface, resulting in less useful sound absorption

The sound energy consumption of sound absorbing materials mainly follows three principles: (1) The air molecules in porous sound absorbing materials vibrate and rub with the hole wall, and the sound energy is converted into heat energy for dissipation; (2) When longitudinal sound waves penetrate porous materials, the air in the pores is periodically compressed and released, resulting in energy consumption in the energy

conversion process; (3) Sound energy is converted into mechanical energy and thermal energy through the resonance of the hole wall. Accordingly, there are three standards for designing sound absorbers: (1) the material should contain a considerable number of pores (such as cavities, channels or voids); (2) The pore size shall be appropriate and interconnected for acoustic wave propagation; (3) There shall be a continuous passage between the inner hole and the outer surface of the material.

1.2.2 Sound absorption materials

There is already an extensive list of sound absorbing materials (SA), however, the development of new sound absorbing materials and structures are still a challenge work. Generally speaking, sound absorbing materials are divided into synthetic and natural. Synthetic sound absorbers are mainly made of polymers and minerals. These sound-absorbing materials are classified into polymer-fiber composites, polymer foams, metal foams, metal fibers, and so on. Single hollow polyester fiber (SHHPF) reinforced hydrogenated carboxylated nitrile rubber (HXNBR) composites have been shown to have excellent sound absorption properties (SAP) [11], and HXNBR/SHHPF is a lightweight composite with excellent acoustic properties. Similarly, the acoustic parameters of PET composites reinforced with carbon fiber and glass fiber, respectively, showed excellent acoustic properties [12]. Likewise, the acoustic properties of nylon 66 scrim-reinforced polyvinyl fluoride (PVF) laminate films and their composite structures with glass fiber mats and carbon fiber boards were investigated [13], and the results showed that by embedding an air layer in the composite, the sound insulation

performance was effectively improved. The polyvinyl alcohol (PVA) and polyethylene oxide (PEO) nanofibrous membranes [14] and their compositions (nanofibrous membranes and needle-punched nonwovens) also demonstrated good sound absorption performance [15].

A variety of foam materials have also been shown to have excellent sound-absorbing properties. They have the unique advantages of high porosity, low density, large surface area and low manufacturing cost. Porous foams are widely used for noise control in areas such as construction and transportation due to their ability to dissipate sound energy over a wide frequency range. Based on the chemical composition of the material, sound-absorbing foams can be divided into three groups: organic foams, hybrid foams, and inorganic foams. Organic foams, exemplified by polyurethane (PU) foams [16], form a cavity and pore structure during the polymerization process, and the cell size is determined by the gelation and foaming reactions. If the cavity pressure is much greater than the wall strength, a foam with an open cell structure can be obtained. Since thicker cavity walls tend to solidify at low drainage flow rates, partial openings will be created if the solidification process completes earlier than the formation of full openings. If the cavity walls are fully solidified before the walls rupture, closed pores will be left.

Hybrid foams are typically obtained by direct blending of fillers with blowing agents, typically using sonication during mixing to avoid filler aggregation. In addition to controlling synthesis conditions, hybrid foams incorporating fibers or particles can also be used to control the microstructure of the cell structure, thereby tuning the sound-absorbing properties of the foam. Efforts have been made to alter the channel structure

of foams, for example, to manufacture foams using various types of fillers, such as natural tea fibers, bamboo leaves, rice husks, alkali-treated wood fibers, and inorganic fillers [17-20].

Inorganic foams have unique properties in terms of physical, mechanical and thermal resistance, which ensure their application in harsh environments [21-22]. They can be prepared by introducing a pore-forming agent (such as polymer particles) during the mixing process and then removing the pore-forming agent by high-temperature sintering, and the pore structure and porosity [23] can be controlled by adjusting the amount of additives. Typically, researchers prepared porous silicon nitride (Si_3N_4) foams by volume-controlled mechanical foaming [24].

1.2.3 Natural sound absorption materials

Although the synthetic sound-absorbing materials have been used widely as noise-absorbing materials, but they have disadvantages such as health problems and pollution to users. In contrast, natural fibers have biodegradable and environmentally friendly synthetic processes. Various studies have been conducted to develop new environmentally friendly sound absorption materials. The sound-absorbing and sound-transmitting properties of bio-based materials and unconventional sustainable natural or recycled building insulation have been studied [25]. Information on natural absorbents such as wood, coconut husk, tea, loofah, jute, flax, kenaf, hemp, palm, rice husk, *etc*. [26-28], has been reported in many literatures. In addition, the acoustic properties of natural fibers such as kenaf, wood, mineralized wood, hemp, palm, date,

cork, sugar cane, cardboard, etc.[29], have shown good sound absorption performance especially in the mid-high frequency range. Many studies have been carried out on coir-based acoustic materials. The sound absorption capacity of natural coir and the flame retardant properties of coir sound-absorbing panels in compliance with building standards were also investigated.

In addition to being green and pollution-free, using natural raw materials as sound-absorbing materials has been focused. Growing plants can be used directly as sound absorbers, such as vertical greening systems. Making virgin natural fiber sound absorbers consumes less energy, has a lower carbon footprint, and is more environmentally friendly than well-processed fiber sound absorbers. In addition, due to the diversity of natural fiber raw materials in nature, acoustic properties are more likely, and their acoustic properties do not remain stable all the time due to variety and in-homogeneity. Therefore, it is not easy to accurately predict the acoustic performance of raw materials.

1.3 Sound reduction structure

The combination of a board, an air layer, and/or a porous material, when the board has a sealed air layer behind it, forms a resonant vibration mechanism in which the mass of the board is supported by an air spring [30]. When sound waves near the resonant frequency enter the board, the sound energy is consumed as vibration energy in the vibration system, and sound absorption occurs. In architecture, wood plywood, plasterboard, and plastic board are usually used as board materials.

Porous materials are mainly used to absorb sound waves in the mid to high-frequency range, while plates and perforated plates are used to absorb sound mainly at specific frequencies in the low to mid-frequency range. By utilizing the sound absorption characteristics of each material and by changing the combination and dimensions of each material and its structure, it is now possible to design structure with a certain level of sound absorption frequency characteristics. Porous materials with continuous pores, such as glass wool, are helpful as sound-absorbing materials because of their high sound-absorption performance. Reusing biomass leads to carbon fixation and is carbon neutral even if it is incinerated afterwards. From the viewpoint of global environmental protection, the materials that compose sound-absorbing materials are also attracting attention. For example, the materials made of recycled construction waste and biomass. This is because their reuse leads to the realization of a low-carbon and recycling-oriented society. In addition, the required added value of sound-absorbing materials changes depending on the location where they are used. For outdoor use, weather resistance, water resistance, and washability are required, while for indoor use, design, heat insulation, and fire resistance are required. There are many demands for sound-absorbing materials, but in any case, it is necessary to develop sound-absorbing materials that meet the needs of the times.

1.4 Purpose and significance of the research

1.4.1 Research purpose

The noise increased considerably in current environments. The situation is getting

worse and worse all the time since the noise increases with the population. Nowadays, with the rapid growth of the modern industrial process, human beings usually suffer from serious problems induced by noise pollution, which has caused considerable harm to physical and mental health, including tinnitus, annoyance, sleep disturbance, or even ischemic heart disease.

The sound absorption technique is a method for noise control. Many researchers have demonstrated that combining designs provide different sound-absorbing properties than single structures employing porous sound-absorbing materials. It is difficult to theoretically predict the sound absorption characteristics of a composite structure and to adjust the acoustic resistance part of such constructions. Porous structures with good low-frequency sound absorption and a small thickness are crucial for effective noise reduction. The exploration of high-efficiency technologies for controlling noise from the living environment is significant. Developing advanced sound absorption materials and structures is an effective method to solve these problems.

The purpose of this research is to develop a new sound absorbing device with excellent sound absorption performance as countermeasures against noise problems. We investigated the sound absorption effect of functional materials and established a performance evaluation system to clarify the mechanism of sound propagating process and sound absorption. In particular, we produced a sound-absorbing structure using natural materials containing waste materials and natural fibers to challenging a new design of sound-absorbing material.

1.4.2 Research Significance

We proposed a new absorbing device, a double cavity resonant device (DCRD), with multi-band sound absorption characteristics. To form the sound absorption structure with two air cavities, a sound-absorbing material designed to be inserted in the neck of the DCRD and a microperforated board is inside the Helmholtz resonator. The sound absorption mechanisms are discussed systematically. In addition, a laminated sound-absorbing structure using natural straw and rice husk was designed, and the reasonable absorption performance is obtained.

1.5 Outline of dissertation

In this work, we developed a new sound absorbing device with excellent sound absorption performance for noise problems. The sound absorption effect of the developed structure and the mechanism of sound wave propagation is investigated. In addition, a laminated sound-absorbing structure using natural straw and rice husk was designed. Based on the above research process, this dissertation is organized by five chapters.

In chapter 1, an overview of sound absorption materials and structures are discussed.

In chapter 2, we proposed a single cavity resonant device (SCRD) and a new double cavity resonant device (DCRD) with multi-band sound absorption

characteristics. Two air cavities with a sound-absorbing material in the neck of the DCRD and a microperforated board inside the Helmholtz resonator are designed. The absorption coefficients and peak frequencies are systematically discussed.

In chapter 3, the sound absorbing characteristics of the DCRD with the insertion of various sound-absorbing porous materials combining MPPs are investigated. The results reveal that the sound absorption performance of DCRD is more than twice that of the Helmholtz resonance structure. And the developed DCRD could almost absorb low-frequency sounds without sacrificing high-frequency performance with the insertion of MPPs.

In chapter 4, a laminated sound-absorbing structure using natural straw and rice husk is designed. By classifying the rice straw into different groups, their sound absorption characteristics were evaluated and optimized. It was found that a multi-layered sound absorbing structure consisting of perforated MDF plates and samples of thick rice straw and rice hulls has better sound absorption performance on the low frequency side than a multi-layered sound absorbing structure using non-woven fabric.

In chapter 5, a summary of this work and conclusions were presented.

Reference

[1] Morillas JMB, Gozalo GR, González DM, Moraga PA, Vílchez-Gómez R. Noise pollution and urban planning. Curr Pollution Rep 2018;4:208–19.

[2] Geravandi S, Takdastan A, Zallaghi E, Vousoghi Niri M, Mohammadi MJ, saki H, et al. Noise pollution and health effects. Jundishapur J Health Sci 2015;7.

[3] Ma J, Li C, Kwan M-P, Chai Y. A multilevel analysis of perceived noise pollution, geographic contexts and mental health in beijing. IJERPH 2018;15:1479.

[4] Yasumoto S, Nakaya T, Jones AP. Quantitative environmental equity analysis of perceived accessibility to urban parks in osaka prefecture, japan. Appl Spatial Analysis 2021;14:337–54.

[5] Wang D, Ying L, Jia Y, Zhang L, Zhang F, Wang W. Noise pollution mitigation method for substations in urban communities based on a smart silencing unit. Journal of Cleaner Production 2020;245:118911.

[6] Persson Waye K, Smith MG, Hussain-Alkhateeb L, Koopman A, Ögren M, Peris E, et al. Assessing the exposure-response relationship of sleep disturbance and vibration in field and laboratory settings. Environmental Pollution 2019;245:558–67.

[7] Bujoreanu C, Nedeff F, Benchea M, Agop M. Experimental and theoretical considerations on sound absorption performance of waste materials including the effect of backing plates. Applied Acoustics 2017;119:88–93.

[8] Rahimabady M, Statharas EC, Yao K, Sharifzadeh Mirshekarloo M, Chen S, Tay FEH. Hybrid local piezoelectric and conductive functions for high performance airborne sound absorption. Appl Phys Lett 2017;111:241601.

[9] Peng L, Song B, Wang J, Wang D. Mechanic and acoustic properties of the sound-absorbing material made from natural fiber and polyester. Advances in Materials Science and Engineering 2015;2015:1–5.

[10] Yang M, Sheng P. Sound absorption structures: from porous media to acoustic metamaterials. Annu Rev Mater Res 2017;47:83–114.

[11] Jie H, Sheng J, Xiong Y. Sound absorption properties of single-hole hollow polyester fiber reinforced hydrogenated carboxyl nitrile rubber composites. Autex Research Journal 2017;17:263–7.

[12] Mehdi Jalili M, Yahya Mousavi S, Pirayeshfar AS. Investigating the acoustical properties of carbon fiber-, glass fiber-, and hemp fiber-reinforced polyester composites. Polym Compos 2014;35:2103–11.

[13] Chen L, Chen Z, Zhang X, Wang W. Sound insulation property study on nylon 66 scrim reinforced PVF laminated membranes and their composite sound proof structure. IOP Conf Ser: Earth Environ Sci 2018;108:022029.

[14] Liu H, Zuo B. Structure and sound absorption properties of spiral vane electrospun PVA/PEO nanofiber membranes. Applied Sciences 2018;8:296.

[15] Abdul Latif H, Yahya MN, Rafiq MN, Sambu M, Ghazali MI, Mohamed Hatta MN. A preliminary study on acoustical performance of oil palm mesocarp natural fiber. AMM 2015;773–774:247–52.

[16] Sung G, Kim SK, Kim JW, Kim JH. Effect of isocyanate molecular structures in fabricating flexible polyurethane foams on sound absorption behavior. Polymer Testing 2016;53:156–64.

[17] Ekici B, Kentli A, Küçük H. Improving sound absorption property of polyurethane foams by adding tea-leaf fibers. Archives of Acoustics 2012;37:515–20.

[18] Chen S, Jiang Y. The acoustic property study of polyurethane foam with addition of bamboo leaves particles. Polym Compos 2018;39:1370–81.

[19] Wang Y, Zhang C, Ren L, Ichchou M, Galland M-A, Bareille O. Influences of rice hull in polyurethane foam on its sound absorption characteristics. Polym Compos 2013;34:1847–55.

[20] Sung G, Kim JW, Kim JH. Fabrication of polyurethane composite foams with magnesium hydroxide filler for improved sound absorption. Journal of Industrial and Engineering Chemistry 2016;44:99–104.

[21] Cheng W, Duan C, Liu P, Lu M. Sound absorption performance of various nickel foam-base multi-layer structures in range of low frequency. Transactions of Nonferrous Metals Society of China 2017;27:1989–95.

[22] Liu PS, Qing HB, Hou HL. Primary investigation on sound absorption performance of highly porous titanium foams. Materials & Design 2015;85:275–81.

[23] Cuiyun D, Guang C, Xinbang X, Peisheng L. Sound absorption characteristics of a high-temperature sintering porous ceramic material. Applied Acoustics 2012;73:865–71.

[24] Wang F, Gu H, Yin J, Xia Y, Zuo K, Liang H, et al. Porous Si3N4 fabrication via volume-controlled foaming and their sound absorption properties. Journal of Alloys and Compounds 2017;727:163–7

[25] Zhu X, Kim B-J, Wang Q, Wu Q. Recent advances in the sound insulation properties of bio-based materials. BioResources 2013;9:1764–86.

[26] Cao L, Fu Q, Si Y, Ding B, Yu J. Porous materials for sound absorption. Composites Communications 2018;10:25–35.

[27] Berardi U, Iannace G. Acoustic characterization of natural fibers for sound absorption applications. Building and Environment 2015;94:840–52.

[28] Hosseini Fouladi M, Ayub Md, Jailani Mohd Nor M. Analysis of coir fiber acoustical characteristics. Applied Acoustics 2011;72:35–42.

[29] Koruk H, Genc G. Investigation of the acoustic properties of bio luffa fiber and composite materials. Materials Letters 2015;157:166–8.

[30] Kim B-S, Park J. Double resonant porous structure backed by air cavity for low frequency sound absorption improvement. Composite Structures 2018;183:545–9.

Chapter 2: Sound absorption performance of SCRD/DCRD

2.1 Introduction

The sound absorption technique is a method for noise control. Generally, the sound absorption coefficient of the sound-absorbing material is tiny in the low-frequency range and significant in the high-frequency range. In other words, at low-frequency, the sound-absorbing effect is generally insufficient. The resonator structure significantly impacts a specific frequency in the mid-low-frequency range. However, the bandwidth of sound absorption is exceptionally narrow. A suitable sound absorption coefficient will not appear unless a porous sound-absorbing material is attached. Absorbent materials are generally employed to reduce noise in various industrial applications. The minimum thickness of a porous absorber should not be less than a quarter wavelength, which can show satisfactory sound absorption performance. For absorption of sound below 500 Hz, the sound absorption material's thickness should be greater than 17 cm theoretically—the low-frequency sound absorption is decided by the porous medium's thickness or the back cavity of air. The preferred thickness is small in practical applications. Many researchers have demonstrated that combining designs provide different sound-absorbing properties than single structures employing porous sound-absorbing materials. Porous structures with good low-frequency sound absorption and a small thickness are crucial for effective noise reduction.

Kim and Park studied the sound absorption in the middle and low-frequency ranges by installing an expansion tube and an effective panel containing a porous sound-

absorbing material in parallel [1-2]. Li proposed a new concept for applying a thin porous layer in low- and medium-frequency sound absorption, which can be employed as an alternative to the microperforated panel (MPP) for low mid-frequency sound absorption. This composite structure is examined in the form of a porous material matrix and a perforated resonator. The perforated resonator is a thin perforated plate filled with porous material (PM) in its back cavity [3-4]. Photiadis DM investigated the sound absorption of a sound-absorbing body in the shape of a resonator by stacking two types of porous sound-absorbing materials and providing a cavity behind them [5]. Based on the Helmholtz resonator, the combined sound absorption mechanism revealed that the Helmholtz resonator with an elastic cavity wall has a lower resonance frequency and availability than the Helmholtz resonator with a rigid cavity wall, Selamet et al. [6]. Tang focused on the Helmholtz resonator's acoustic properties lined with an absorbent material and demonstrated that applying a fibrous material to the inside of the cavity reduces the resonance frequency and shows the maximum sound propagation loss [7].

However, the theory and design of perforated panel sound-absorbing constructions are well established. In contrast, the difficulties in adjusting the acoustic resistance part of such constructions curtail their usefulness. Researchers have become interested in the MPP proposed by Maa, which is used to absorb sound and reduce its intensity [8-11]. MPP has low and medium-frequency sound absorption bandwidths and has a better range of sound absorption effects in resonator and vibration sound absorption materials. To enhance the sound absorption at the low-frequency band and reduce the total thickness, Park studied the acoustic properties of an MPP backed the Helmholtz

resonator structure [12]. These investigations have proposed different sound absorption structures to widen the sound absorption band [13-22]. However, it is difficult to theoretically predict the sound absorption characteristics of a composite structure since it has become more complex. The effect of composite structures on sound absorption characteristics has not been clarified yet in several cases.This chapter discusses a single cavity structure (SCRS) and a double cavity structure (DCRS) embedded with PMs and/or MPPs to enhance low-frequency absorption performance. The sound absorption coefficient of each structure was measured by the vertical incident approach to clarify the parameters' contribution. We discussed the influence of different hole shapes and panel shapes of the single-cavity resonant devices (SCRD) and the different area ratios of the double-cavity resonant device (DCRD) on sound absorption properties. The SCRD's and DCRD's sound absorption characteristics are discussed systematically and compared with single cavity resonant structure (SCRS), the classical Helmholtz resonance (HR) devices, especially in the low-frequency region. The noise suppression effect with an embedded sound absorption material and the Helmholtz resonator structure are discussed in improving low-frequency sound absorption and widening the sound-absorbing band. The result proves that the expected noise suppression effect can be achieved with appropriate material and structure design without increasing the device's thickness.

2.2 Experimental section

2.2.1 Materials

The Helmholtz resonators' partition plate and the microperforated panels (MPPs) are made of medium-density fiberboard, and three types of MPPs are designed by changing their parameters, as listed in Table 2-1. Three different perforation ratios were designed to investigate the effect of MPP design on the acoustic performance of the complex. And three porous materials (PMs, **Fig. 2-1**), including polyurethane wave foam (PUW, area density of 1.48 kg/m^2), polyurethane flat foam (PUF, area density of 1.43 kg/m^2) and glass wool flat foam (GWF, area density of 1.66 kg/m^2) are provided by supplied by FUJIFILM Wako Pure Chemical Corporation, Japan.

Table 2-1 The parameter of the microperforated panels (MPPs)**.**

No.	Panel type	Hole number	Area ratio (%)	Perforation ratio (%)	Hole diameter (mm)
1	MPP 1	158	40	0.61	1
2	MPP 2	316	80	2.42	1
3	MPP 3	632	160	9.69	1

※ MPP composite panels' Main components in the panel were wood fibers, synthetic resin, and wax. The hole diameter was 1 mm. The area ratio is the ratio of the surface area of the holes (MPP) to the cavity (Helmholtz resonator).

※ Area ratio = the total area of small holes in the MPP/neck area of the resonator echo

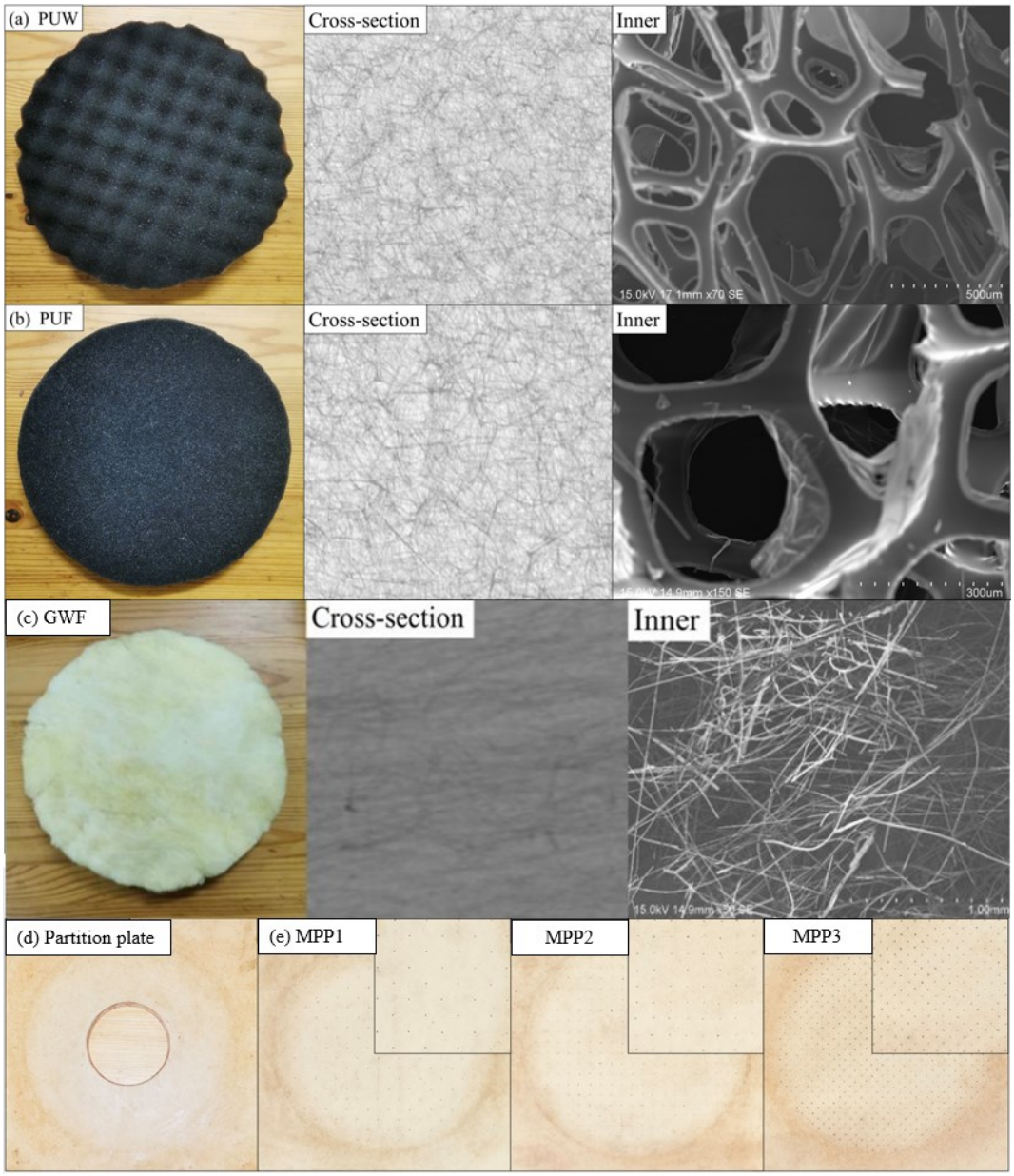

Fig. 2-1. The internal and cross-sectional structures of (a) polyurethane wave foam (PUW), (b) polyurethane flat foam (PUF), (c) glass wool flat foam (GWF), (d) partition plate of the Helmholtz resonators, and (e) microperforated panels (MPPs).

2.2.2 Configuration of the device

Fig. 2-2 shows a diagram of a single cavity resonant device (SCRD). Set a partition plate with a length (l) of 15 mm and cavity diameter (a) of 80 mm at the tube's neck. The shape of the partition plate's neck is circular. Both the partition plate and the closed end of the duct end are rigid bodies. A resonator was formed by the space created between the partition plate and the closed end. By designing two types of single panel-single cavity structures (SCRS) and DCRS, three types of resonant structures are designed to analyze each part's sound absorption characteristics. The composite structures' parameters are illustrated in **Fig. 2-3**. For Sample 1, a PM thickness of 15 mm and a diameter of 80 mm was filled into Helmholtz's neck; for Sample 2, an MPP was inserted to compose a double cavity resonant structure.

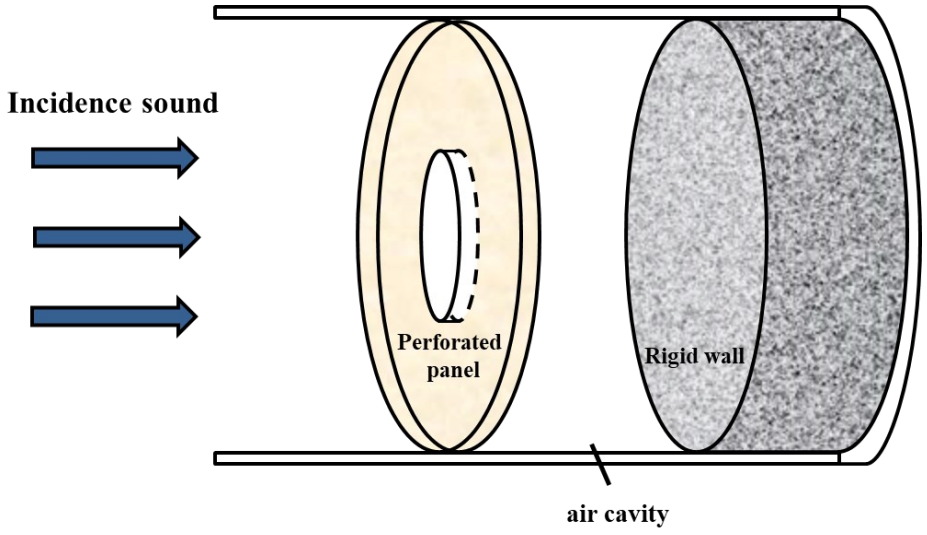

Fig. 2-2. 3D section viewing of the single cavity resonant device (SCRD).

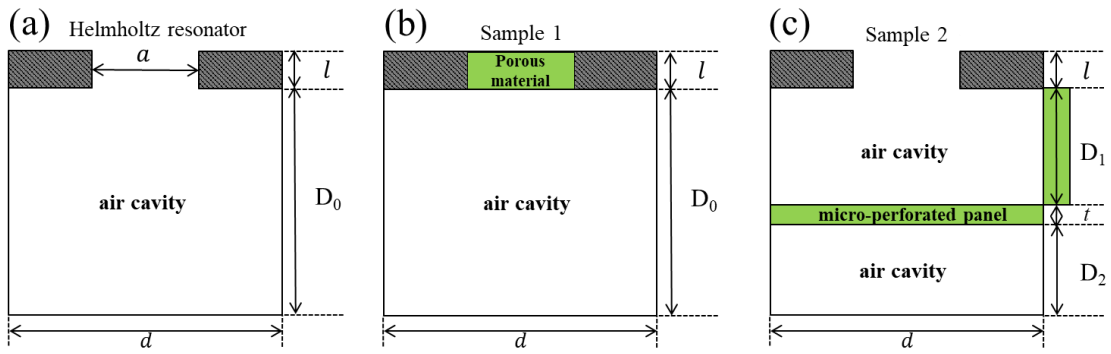

Fig. 2-3. Configurations of (a–b): SCRD, (c): DCRD.

2.2.3 Measurement of normal incidence sound absorption coefficients

The sound absorption coefficient and impedance are measured according to standards of ISO 10534-1 [23] and ISO 10534-2 [24], which can be used to evaluate the sound absorption performance of materials. For normal sound incidence, an impedance tube, two microphone locations, and a digital frequency analysis system are employed together to measure the sound absorption coefficient of sound absorbers. A corresponding schematic diagram of the testing configuration is shown in **Fig. 2-4**. A full-range loudspeaker 20F-20 (Technics), two condenser microphones ISOMAX (COUNTRYMAN) and audio interface Fireface400 (RME) are used for signal generating, sound pressure-field measuring and signal processing. Before the test, the sound-absorbing tube should be straight, and the inside surface should be smooth, nonporous and dust-free to ensure effective sound attenuation.

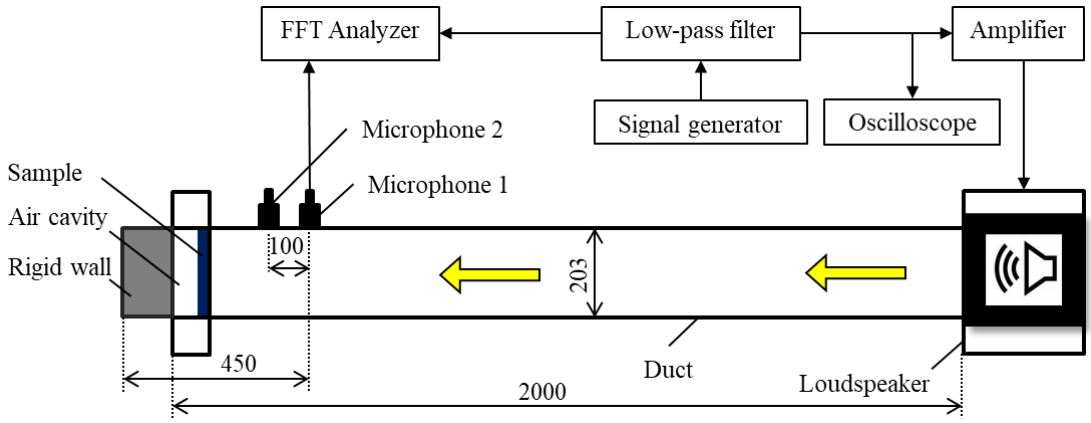

Fig. 2-4. Experimental apparatus for low-frequency sound absorptions.

The normal incidence sound absorption coefficient, α, can be computed using the following Eq. (1) if the sound, I_i, is incident on the sample and the reflected sound, I_r. The minimum value of α is 0, and the maximum is 1, where s represents the distance between microphones 1 and 2, H represents the two microphone signals' transfer function corrected for microphone response mismatch, $H_{12} = P_2/P_1$ and r represents the reflectance coefficient [25].

$$\alpha = 1 - \frac{I_r}{I_i} \tag{2-1}$$

$$r = \frac{H_{12} - e^{-jk_0 s}}{e^{jk_0 s} - H_{12}} e^{2jk_0 x_1} \tag{2-2}$$

$$\alpha = 1 - |r|^2 \tag{2-3}$$

2.2.4 The measurable frequency range of the experimental apparatus

$f_l < f < f_{\mathrm{u}}$ is the working frequency range. The lower frequency limit depends on the microphones' spacing and the analysis system's accuracy. It is recommended that the microphone spacing exceeds 5% of the wavelength corresponding to the lower frequency of interest to perform the plane wave measurements accurately within these frequency limits to avoid cross modes, which occur at higher frequencies when the acoustical wavelength approaches the tube's sectional dimension [24]. Where s, c, and d are the microphone spacing (m), the speed of sound in the tube (m/s), the diameter of the tube (m), respectively, and $K = 0.586$. The lower working frequency and upper-frequency limit of the tube frequency range of the experimental apparatus in the acoustic tube can be computed from the following equation in this experiment [23].

$$f_l > \frac{c}{20s} \tag{2-4}$$

$$f_u < \frac{Kc}{d} \tag{2-5}$$

The experimental apparatus conducted all the tests at 23°C. The tube diameter, d, was 0.203 m, the distance between microphones one and two, s, was 0.01 m, and the sound frequencies that can be precisely measured were in a range of170 Hz<f<970 Hz.

2.2.5 Prediction absorption coefficients of the SCRD and DCRD

The SCRD sample 1's and DCRD sample 2's total acoustic impedance is expressed as [26]

$$\mathrm{Z}_t = Z_{tr} + iZ_{ti} = [Z_{MDF}^{-1} + Z_P^{-1} + Z_{AC}^{-1}]^{-1} \tag{2-6}$$

and

$$\mathrm{Z}_t = Z_{tr} + iZ_{ti} = [Z_{MDF}^{-1} + Z_{MPP}^{-1} + Z_{DAC}^{-1}]^{-1} \tag{2-7}$$

where Z_{MDF}, Z_P, Z_{MPP}, and Z_{AC}, Z_{DAC} represent the acoustic impedances of MDF, porous, MPP, and the air cavity of sample 1 and the double air cavity of the HR sample 2, respectively. The MDF's acoustic impedance was predicted through wave propagation in MDF, as $Z_{MDF} = Z_c \coth(ik_{MDF}l/\rho_0 c_0)$, where ρ_0 represents the density and c_0 represents the wave speed of air. The characteristic impedance, Z_c and wavenumber, k_{MDF} of the MDF were obtained as $Z_c = (\rho_{MDF} K_{MDF})^{0.5}$ and $k_{MDF} = \omega(\rho_{MDF}/K_{MDF})^{0.5}$, respectively. The effective density, ρ_{MDF} and bulk modulus, K_{MDF}, were given as [27]

$$\rho_{MDF} = \rho_0\left[1 + (\delta/a)\sqrt{2/i}\right] \tag{2-8}$$

$$K_{MDF} = \frac{\gamma P_0}{\gamma - (\gamma - 1)/1 + (\delta/Ba)\sqrt{2/i}} \tag{2-9}$$

where γ, B, P_0, and a represent the specific heat ratio, square root of the Prandtl number, atmospheric pressure, and slit thickness, respectively. $\delta = (2\eta/\omega\rho_0)^{0.5}$ is the viscous skin depth, where η represents the shear viscosity.

The acoustic impedance of the PM inserted $Z_P = Z_c coth\gamma l$. The characteristic impedance, Z_c, and specific acoustic resistance, γ, of the porous was obtained as $Z_c = R + jX$ and $\gamma = \alpha + j\beta$, respectively, which were given as [28]

$$Z_c = 1 + 0.070\left(\frac{f}{R}\right)^{-0.632} + i\,0.107\left(\frac{f}{R}\right)^{-0.632} \tag{2-10}$$

$$\gamma = k\left\{0.160\left(\frac{f}{R}\right)^{-0.618}\right\} + ik\left\{1 + 0.109\left(\frac{f}{R}\right)^{-0.618}\right\} \tag{2-11}$$

where $R\ and\ \alpha$ represent the specific acoustic resistance and the absorption coefficient of the porous.

The acoustic impedance of the MPP inserted $Z_{MPP} = r + j\omega m,$ the normalized specific acoustic resistance of r and ωm were given as [29]

$$r = \frac{32\eta t}{p\rho_0 c_0 d^2}\left(\sqrt{1 + \frac{k^2}{32}} + \frac{\sqrt{2}}{32}k\frac{d}{t}\right) \tag{2-12}$$

$$\omega m = \frac{\omega t}{pc_0}\left(1 + \frac{1}{\sqrt{9 + \frac{k^2}{2}}} + 0.85\frac{d}{t}\right) \tag{2-13}$$

$$k = d\sqrt{\frac{\omega\rho_0}{4\eta}} \tag{2-14}$$

where ρ_0, $c_0, t, d,$ and p represent the density of air, the sound velocity in air, the thickness (mm), the aperture diameter (mm), and the aperture ratio of MPP, respectively.

The acoustic impedance of the double air cavity inserted $Z_{DAC} = [\ Z_{NAC}^{-1} + Z_{PAC}^{-1} + Z_{MAC}^{-1}]^{-1}$. Z_{NAC} is the acoustic impedance of the air space in HR's neck. D_1 represents the depth of the air cavity between PM and MMP, D_2 represents the depth of the air cavity between MPP and rigid wall. The acoustic impedance,Z_{PAC}, Z_{MAC}, of the air space were obtained as $Z_{PAC} = icotkD_1$ and $Z_{MAC} = icotkD_2$, respectively. The predicted sound absorption coefficient α for the DCRD was expressed as follows，

$$\alpha = \frac{4Z_{tr}}{(1 + Z_{tr})^2 + Z_{ti}^2} \tag{2-15}$$

2.3 Results and discussion

2.3.1 Performance of the PMs

Fig. 2-5a demonstrates how the sound wave in PMs propagates through the frames, voids, and pores. Incident sounds are transmitted from the air into the PM. The media through which the sound waves propagate are the micro-pores and gaps of PM and its air. The sound wave is incident vertically to the PM's surface. The material's surface reflects that part of it. The other part is transmitted to the inside of the material through the hole connected with the outside world. The acoustic wave's vibration into the material causes violent movement of the air inside the through-hole, causing it to rub

against the hole-wall. Part of the sound energy is converted into heat energy under friction and viscous force, which attenuates the sound waves and weakens the reflected sound energy to achieve sound absorption. Furthermore, the heat exchange between the air and the entire wall and the material causes heat loss, which causes sound energy attenuation.

The normal incidence sound absorption coefficients of three porous materials, PUW, PUF and GWF, are measured without the resonator, as shown in **Figs. 2-5b c** and **d,** and Table 2-2. The thickness was 15 mm, a diameter of 203 mm, the surface densities were 1.48, 1.43 and 1.66 kg/m^2, and the air cavity depths were 0, 16, and 32 mm, respectively, and the other design parameters were kept constant. Firstly, the sound absorption coefficient of the similar surface densities but different panel shapes for the continuous round hole materials. PUW and PUF are evaluated without the resonator (**Fig. 2-5b**, **Fig. 2-5c**). Clearly, it can be found that both PUW and PUF showed increased sound absorption capacity, approximately twice as much, with the increase of D_0 from 0 to 32 mm. Especially the increase is dramatic in the high-frequency acoustic region (>900 Hz). This is because the cavity structure inside PUF is more compact, which improves the resonant frequency of high-energy sound waves to induce it to refract back and forth in the spot many times, resulting in whole wall friction of energy conversation. In addition, the sound absorption coefficient of PUF is higher than PUW in the relatively high-frequency region of less than 900 Hz.

For the sound absorption coefficient of flat foam different hole shapes (**Fig. 2-5c**, **Fig. 2-5d**), GWF is better than PUF in the frequency region of less than about 900 Hz under the same material volume and similar surface densities. The absorption coefficient increased twice for both PMs when the air cavity depth (cavity volume)

changed from 0 to 32 mm. The sound absorption coefficient of PUF increased sharply in the relatively high-frequency region of greater than 900 Hz. The sound waves propagated through the hole structure of the PUF may make the sound refract back and forth in the spot, resulting in the wall friction of energy conversation and improving the resonant frequency. This was because PUF foam has the lowest surface density and higher material permeability than glass fiber and greater air friction between the air in the circular holes inside the material and the cavity walls than in the fibrous GWF and PUW. The more heat exchange between the air and the entire wall causes more heat transfer loss, and a higher absorption rate was obtained.

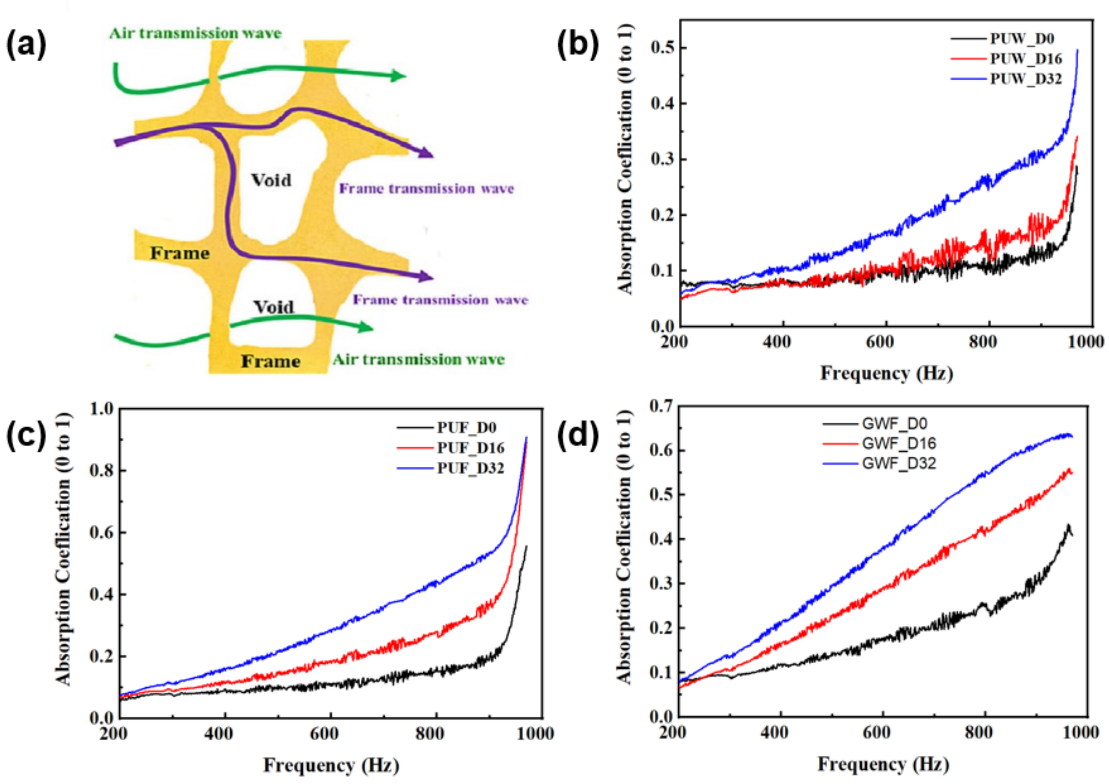

Fig. 2-5. (a) Demonstrates of the sound wave in PMs propagates, measured absorption coefficients of (b) PUW, (c) PUF and (d) GWF.

Table 2-2 Normal incidence sound absorption coefficients of PMs.

No.	Panel type	Air gap 0 (mm)	Air gap 16 (mm)	Air gap 32 (mm)
1	Urethane wave foam	0.27	0.34	0.49
2	Urethane flat foam	0.55	0.89	0.91
3	Glass wool flat foam	0.42	0.55	0.64

2.3.2 Performance of the SCRD with PMs

As shown in **Fig. 2-6**, we embed the PMs into the HR and characterize the sound-absorbing performance of this assembled SCRD. Compared with the SCRD sample without PMs, the peaks of the sound absorption coefficient vary from a larger value of 495.0 Hz to 400.4 (PUF) and 428.7 Hz (PUW), respectively. It means the filling of PMs will make the sound-absorbing vocal fold shift to the low-frequency region, that is, SCRD can play a very good role in the absorption and noise reduction of the low-frequency band sound. Besides, for the SCRD samples with/without PMs, the sound coefficients also exhibit an enhancement from 0.46 to 0.97 (PUF), 0.99 (PUW), corresponding to the increase of sound coefficients (without Hits resonator), which were 0.88 (PUF) and 0.64 (PUW) respectively, indicating that the use of PMs greatly enhanced the acoustic performance of HR. It should be noted that PUF-filled SCRD samples also exhibit the highest sound-absorption coefficients like before. We believe that in addition to the features of lower surface density and higher material permeability for PUF, the friction between the circular hole in the material and the air in the cavity wall is also higher than that of GWF, which can consume more acoustic energy.

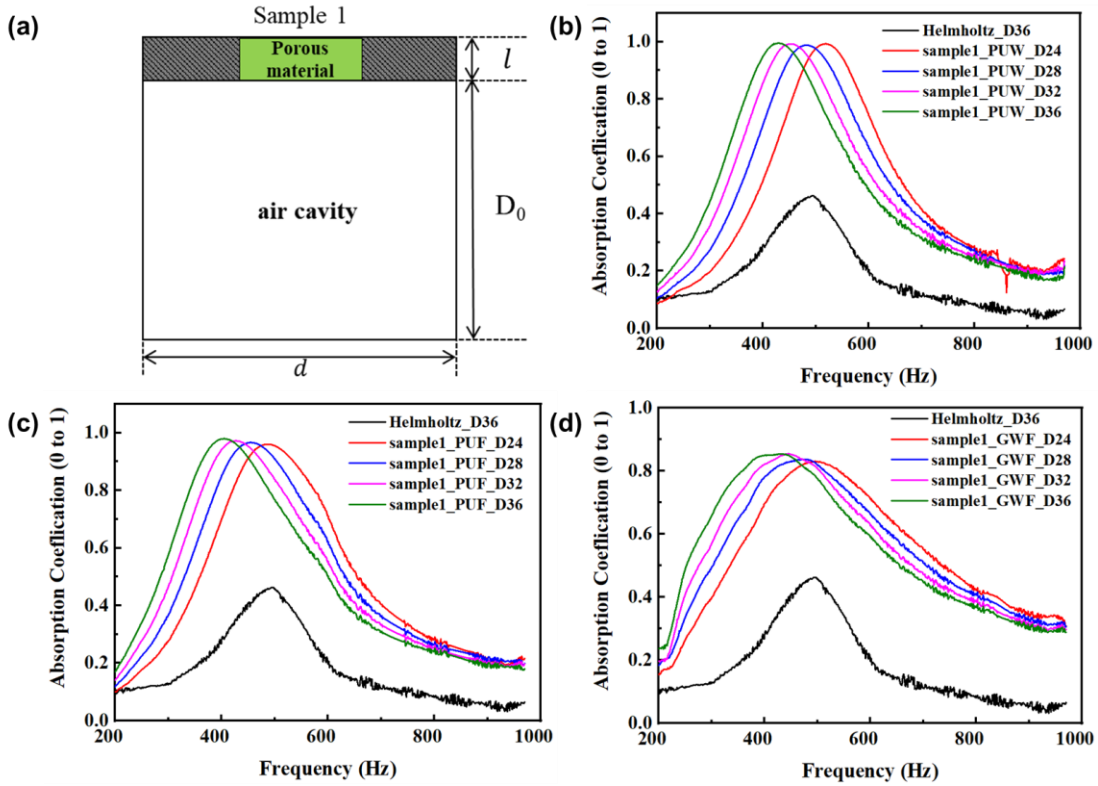

Fig. 2-6. Configurations of (a) Sample 1 (SCRD) and it's (b-d) measured absorption coefficients. The depth of the Helmholtz resonator = 36 mm, air cavity depth 24 mm≦ D≦36 mm, and other design parameters were kept constant for the tested sample.

2.3.3 Performance of the MPPs

Fig.2-7a illustrates the image of sound reflection and absorption in MPP. Incident sound is transmitted from the air into the MPP, causing reflection and absorption. For the MPP plane in the sound pipe, the sound was repelled according to the reflectivity of that surface. It becomes more notable as the frequency decreases. The reflected energy will be reduced depending on the returned echoes. The multiple reflections will

be repeated between surfaces, and incidence, reflection, rotation, and absorption occur on one surface, resulting in two parts of energy, reflected and absorbed energy.

Increasing the number of holes in a fixed area ratio reduces the distance between holes. The mutual friction and reflection of the air around the holes are increased when the sound waves pass through the MPPs, which may enhance sound absorption. For the same thickness and hole diameter, the normal incidence sound absorption coefficients for different area ratios of MPP are illustrated in **Figs. 2-7b–d** to discuss the effect of different MPP designs. Satisfactory sound absorption performance is confirmed when the minimum thickness of the MPP is not less than a quarter wavelength. For MPP1 (**Fig. 2-7b**) with the area ratio of 0.4, when the air depth D = 4, the peak frequency appeared at 600 Hz with an absorption coefficient of 0.48, and when the air depth D changed to 16, 30, and 50 mm, respectively, the peak frequency is decreased to 500, 470, and 440 Hz with the absorption coefficients of 0.75, 0.85, and 0.8, respectively. However, for MPP2 (**Fig. 2-7c**) and MPP3 (**Fig. 2-7d**) with the area ratio of 0.8 and 1.6, respectively, two frequency peaks are observed. The area ratio of MPP has a visible influence on the values of peak frequency and its absorption coefficients, as shown in Table 4. The air depth D also has a great contribution to both peak frequency and the related absorption coefficients and with the increment of the area ratio, the influence of the air depth becomes much more obvious.

When the minimum thickness of MPP is not less than a quarter wavelength, it can show a preferred sound absorption performance. Take MPP1 sample with an area ratio of 0.4 as an example (**Fig. 7b**), the peak frequency appears at 603.2 Hz with the air depth of 4 mm, and the sound absorption coefficient is 0.42. This peak frequency will

be reduced to 481.5 Hz, 462.1 Hz and 438.4 Hz, respectively when cavity depth is increased to 16, 30 and 50 mm. And the absorption coefficients also increase to 0.76, 0.83 and 0.82. However, when the area ratio is further increased to 0.8 and 1.6, it can be observed that the area ratio shows a very large impact on the sound absorption coefficient and peak frequency. They are listed in **Table 2-3**, including the shift of the peak value to the small frequency region and the increasing sound absorption coefficient. Also, it is certain that the unprecedented depth increase always has an improved effect on sound absorption performance.

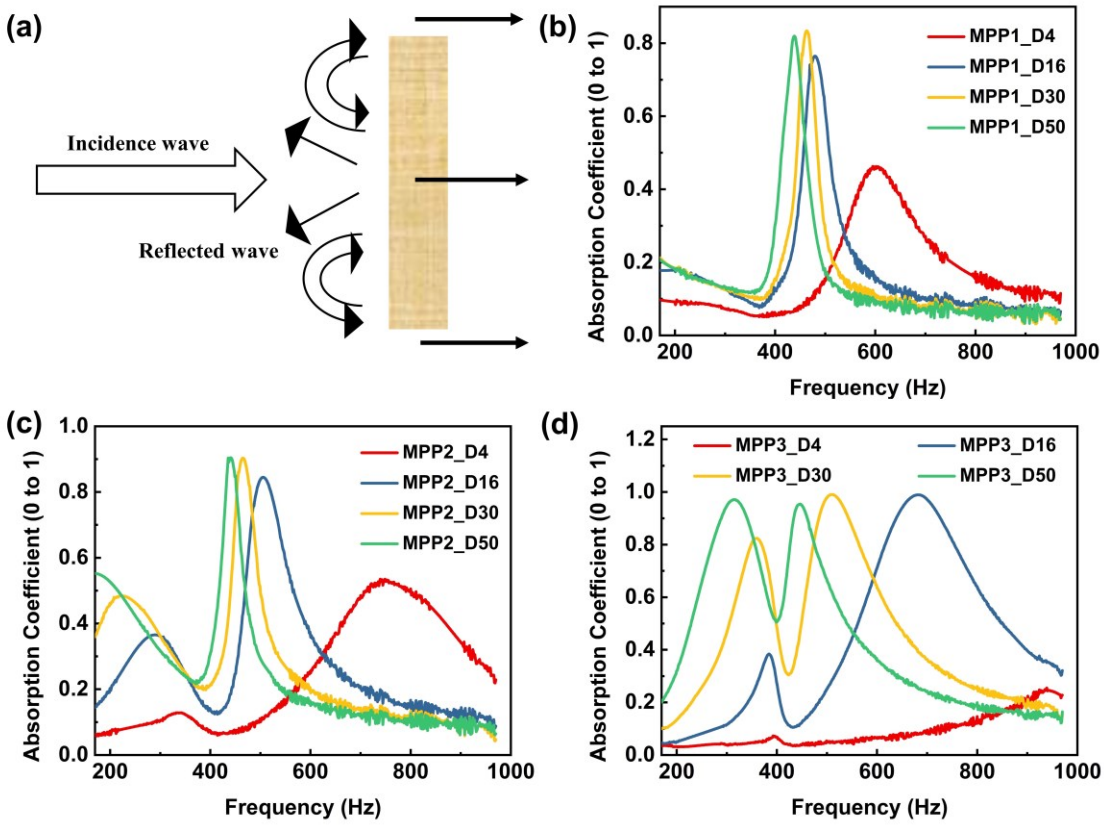

Fig. 2-7. (a) Schematic representation for the acoustic reflection and absorption of MPP. (b-d): Measured absorption coefficients of MPPs. The area ratio of MPPs were 0.4, 0.8, and 1.6, the perforation ratio of MPPs were 0.61, 2.42, and 9.69%, respectively. The

thickness of MPP was 4 mm, and air cavity depths were 4, 16 mm, 30 mm, and 50 mm, respectively. Other design parameters were kept constant for the tested samples.

Table 2-3 Normal incidence sound absorption coefficients of MPPs.

No.	Panel type	Air cavity depth (mm)	MPP area ratio (%)	Peak 1		Peak 2	
				f(Hz)	*a*	*f*(Hz)	*a*
1	MPP1	4	40	601	0.46	-	-
2	MPP1	16	40	480	0.76	-	-
3	MPP1	30	40	461	0.85	-	-
4	MPP1	50	40	438	0.82	-	-
5	MPP2	4	80	739	0.53	-	-
6	MPP2	16	80	290	0.36	505	0.85
7	MPP2	30	80	232	0.49	465	0.90
8	MPP2	50	80	175	0.55	441	0.90
9	MPP3	4	160	960	0.27	-	-
10	MPP3	16	160	384	0.38	678	0.99
11	MPP3	30	160	357	0.82	509	0.99
12	MPP3	50	160	314	0.97	446	0.95

2.3.4 Performance of the DCRD with MPPs

Three different area ratios of the MPPs were designed to investigate the effect of MPP design on the acoustic performance of the DCRD, and their acoustic performance was measured, as illustrated in **Fig. 2-8**. These peaks seem to correspond to the combining vibration modes of 1st, 2nd and 3rd, while the porous materials and MPP resulted in the combination effect on these peaks. Three frequency peaks appeared within the measured frequency region of 170-970 Hz. When the area ratios of MPP1 and MPP2 were 0.4 and 0.8, the sound absorption coefficients at Peak 1 of frequency of around 220 Hz were almost the same with the values of 0.49 and 0.47, respectively.

However, when the area ratio of MPP3 is 1.6, the sound absorption coefficient at Peak 1, about 350 Hz, is enhanced to 0.85, 77% up. The frequency peak moved to the relatively high-frequency side by increasing the area ratio from 0.4 to 1.6. At Peak 2, about 445 Hz, the sound absorption coefficient was around 0.8, showing similar values of the sound absorption coefficient. However, at Peak 3, the frequency shifts to a relatively high-frequency with a large difference of 770, 800, and 950 Hz, corresponding to the area ratio change. The related sound absorption coefficients varied from 1.0 to 0.7 to 0.45.

The results show the acoustic performance and sound absorption coefficient of SCRD assembled by MPPs with different area ratios. The selected cavity depths are 4 mm, 8 mm, 12 mm and 16 mm in turn. Sample 2_MPP1, with an area ratio of 0.4, has two peaks of sound absorption coefficient at 420 Hz and 700-900 Hz, respectively, and the peak intensity fluctuated between 0.9-0.6. In particular, the peak migration trend is the same as the above example; with the increase of cavity depth, the peak shifts toward the low-frequency region, accompanied by increased intensity. However, the second peak frequency changes significantly from 950 to 700 Hz shifting to the low-frequency side with the increment of sound absorption coefficients from 0.35 to 0.8 (more than two times) when the air depths extended from 4 mm to 16 mm. While, for the samples with a high area ratio (0.8 and 1.6), the new peak appears in the low-frequency region of 200-400 Hz, indicating that the assembled SCRD can also have good absorption and consumption of low-frequency sound energy. The absorption performance of different perforation ratios had a massive effect on the area ratio, resonance frequency and peak frequency changes.

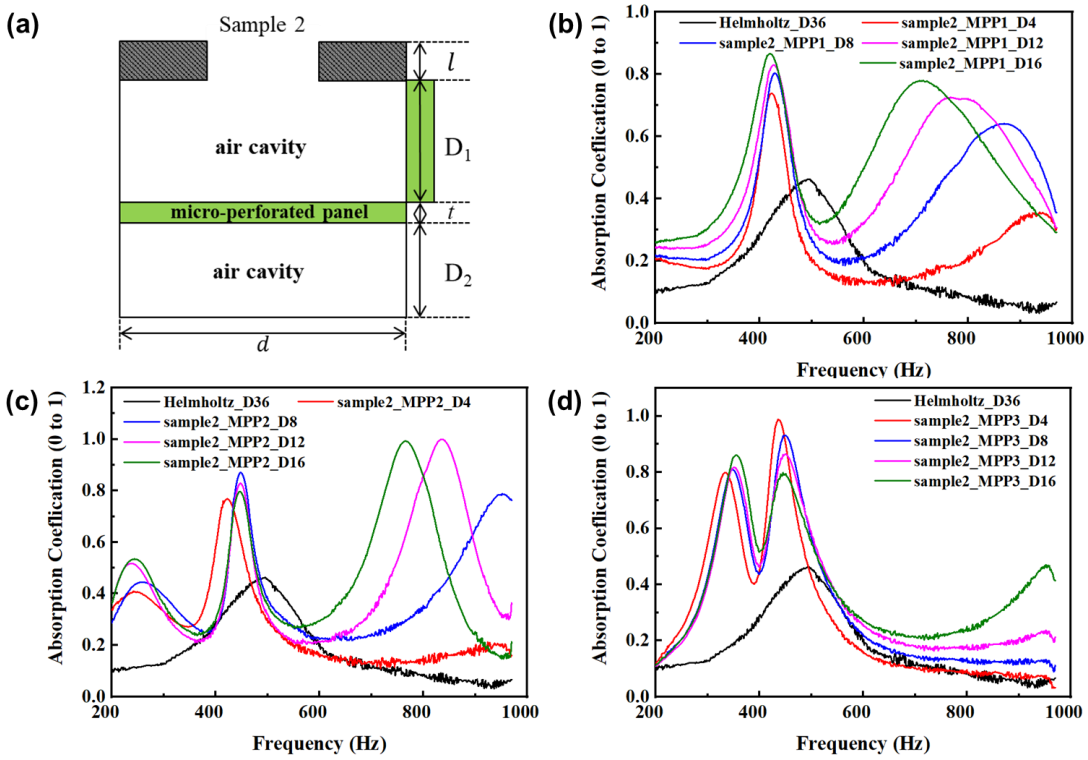

Fig. 2-8. Configurations of (a) Sample 2 (DCRS) and its (b-d) measured absorption coefficients. The area ratio of MPP = (a) 0.4, (b) 0.8, (c) 1.6, the perforation ratio of MPPs were 0.61, 2.42, and 9.69%, respectively. The depth of the Helmholtz resonator = 36 mm, air cavity depth 4 mm ≦ D1 ≦ 16 mm, D2 = 15 mm, and other design parameters were kept constant for the tested sample.

2.4 Conclusion

In this chapter, we proposed a single cavity structure (SCRS) and a double cavity structure (DCRS) embedded with PMs and/or MPPs to enhance low-frequency absorption performance. A new sound absorption structure with two air cavities combining with a porous material or a microperforated board inside the Helmholtz resonator was designed and fabricated. Then, the absorption coefficients and peak frequencies are systematically discussed. The findings revealed that the DCRD's sound

absorption performance is more than two times higher than that of the Helmholtz resonance structure. The developed DCRD could almost absorb low-frequency sounds without sacrificing high-frequency performance by using the microperforated board of MPP 3. The optimization of absorption behavior is obtained, especially in the low-frequency region, which may offer a flexible design approach without increasing the structure's size. In addition, it is clarified that the absorption effect of SCRD with wave foam is better than that of flat foam, and the continuous round hole shape is better than slit holes.

References

[1] Bo-Seung Kim, Junhong Park. Double resonant porous structure backed by air cavity for low frequency sound absorption improvement. Composite Structures 183, 545-549 (2018).

[2] Bo-Seung Kim, Semin Kwon, Seongyoung Jeong, Junhong Park. Semi-active control of smart porous structure for sound absorption enhancement. Journal of Intelligent Material Systems and Structures 1-6 (2019).

[3] Dengke Li, Daoqing Chang, Bilong Liu. Enhanced low- to mid-frequency sound absorption using parallel arranged perforated plates with extended tubes and porous material. Applied Acoustic 127, 316-323 (2017).

[4] Dengke Li, Daoqing Chang, Bilong Liu. Diffuse Sound Absorptive Properties of Parallel-Arranged Perforated Plates with Extended Tubes and Porous Materials. Materials 13(5), 1091 (2020).

[5] Douglas M. Photiadi. The effect of wall elasticity on the properties of a Helmholtz resonator. Journal of the Acoustical Society of America 90, 1188 (1991).

[6] A. Selamet, M. B. Xu, and I.-J. Lee. Helmholtz resonator lined with absorbing material. Journal of the Acoustical Society of America 117, 725 (2005).

[7] Shaokun Tang. On Helmholtz resonators with tapered necks. Journal of Sound and Vibration 279, 1085–96 (2005).

[8] Dah-You Maa. Theory and design of microperforated panel sound-absorbing constructions. Scientia Sinica 18, 55-71 (1975).

[9] Dah-You Maa. Microperforated-panel wideband absorber. Noise Control 29, 77-84 (1987).

[10] Dah-You Maa. Potential of microperforated panel absorber. Journal of the Acoustical Society of America 104, 2861 (1998).

[11] Dah-You Maa. Practical single MPP absorber. International Journal of Acoustics and Vibration 12, pp. 3-6 (2007).

[12] Soon-Hong Park. Acoustic properties of micro-perforated panel absorbers backed by Helmholtz resonators for the improvement of low-frequency sound absorption. Journal of Sound and Vibration 332, 4895-4911 (2013).

[13] Kimihiro Sakagami, Masayuki Morimoto and Wakana Koike. A numerical study of double-leaf microperforated panel absorbers. Applied Acoustics 67, 609-619 (2006).

[14] Kimihiro Sakagami, Tomohito Nakamori, Masayuki Morimoto, Motoki Yairi. Double-leaf microperforated panel space absorbers: A revised theory and detailed analysis. Applied Acoustics 70, 703-709 (2009).

[15] Kimihiro Sakagami, Yoshiki Nagayama, Masayuki Morimoto, Motoki Yairi. Pilot study on wideband sound absorber obtained by combination of two different microperforated panel (MPP) absorbers. Journal of the Acoustical Society of Japan 30, 154-156 (2009).

[16] Kimihiro Sakagami, Ippei Yamashita, Motoki Yairi, Masayuki Morimoto. Sound absorption characteristics of a honeycomb-backed microperforated panel absorber: Revised theory and experimental validation. Noise Control 58(2), 157-162 (2010).

[17] Kimihiro Sakagami, Tomohito Nakamori, Masayuki Morimoto, Motoki Yairi. Sound absorption of a double-leaf micro-perforated panel with an air-back cavity and a rigid-back wall: Detailed analysis with a Helmholtz–Kirchhoff integral formulation. Applied Acoustics 71, 411-417 (2010).

[18] Xin Li, Bilong Liu, Chong Qin. A perforated plate with stepwise apertures for low frequency sound absorption. Applied Sciences 11, 6180 (2021).

[19] Min Yang, Shuyu Chen, Caixing Fu, Ping Sheng. Optimal sound-absorbing structure. Materials Horizons 4, 673-680 (2017).

[20] Zhiling Zhou, Sibo Huang, Dongting Li, Jie Zhu, Yong Li. Broadband impedance modulation via non-local acoustic metamaterials. National Science Review 9, nwab171 (2022).

[21] Hua Ding, Nengyin Wang, Sheng Qiu, Sibo Huang, Zhiling Zhou, Chengcheng Zhou, Bin Jia, Yong Li. Broadband acoustic meta-liner with metal foam approaching causality-governed minimal thickness. International Journal of Mechanical Sciences 232, 107601 (2022).

[22] Ryousuke Mitsuhashi, Tatsuya Morishita. Design of sound absorbing device using resonator and absorbing materials. Symposium on Environmental Engineering 24,103 (2014).

[23] Standard ISO 10534-1. Acoustics－ Determination of sound absorption coefficient and impedance in impedance tubes Part 1：Method using standing wave ratio;1998.

[24] Standard ISO 10534-2. Acoustics－Determination of sound absorption coefficient and impedance in impedance tubes Part 2：Transfer-function method;1998.

[25] Standard ASTM E1050-98. Standard test method for impedance and absorption of acoustical materials using a tube, two microphones and a digital frequency analysis system;1998.

[26] Lawrence E. Kinsler, Austin R. Frey, Alan B. Coppens, James V. Sanders. Fundamentals of acoustics 4th ed. Wiley-VCH; 1999.

[27] Jean F. Allard, Noureddine Atalla. Propagation of sound in porous media: modelling sound absorbing materials. 2nd ed. John Wiley and Sons; 2009.

[28] Yasushi Miki. Acoustical properties of porous materials–Modifications of Delany-Bazley methods–. Journal of the Acoustical Society of Japan 11, 19- 24 (1990).

[29] Chenxi Li, Ben Cazzolato, Anthony Zander. Acoustic impedance of micro perforated membranes: velocity continuity condition at the perforation boundary. The Journal of the Acoustical Society of America 139: 93–103(2016).

Chapter 3: Improved DCRD enhanced with both PMs and MPPs

3.1 Introduction

Nowadays, with the rapid modern industrial process growth, human beings usually suffer from serious problems induced by noise pollution, causing considerable harm to physical and mental health, including tinnitus, annoyance, sleep disturbance, or even ischemic heart disease. Thereby, exploring highly efficient technologies to control noise from the living environment is of great significance [1-3]. Developing advanced sound absorption materials is an effective method to solve these problems [4-8].

Traditional acoustic absorption or noise-reducing materials are mostly porous materials (PMs) [9-12] composed of channels, cracks, or cavities, which usually fall into two broad categories [13-16]: i) fiber-based and ii) foam-based sound-absorbing materials and have been widely used in the architectural acoustic field. When sound waves enter the materials, sound energy is dissipated by thermal loss caused by the friction of air molecules with the pore walls and viscous loss brought by the viscosity of airflow within the materials [17]. These energy consumption principles endow PMs with broad frequency bands for sound absorption. However, leaving aside the relatively complex process of forming porous structures, these high-energy-consumption and petrochemical products still need to be introduced by extra chemical reagents, including adhesives and foaming agents [18]. However, these reagents are not beneficial to the environment and human health. In addition, a single PM usually exhibits good

absorption of sound waves with a high frequency but poor absorption behaviors for sound waves with a low frequency [19-20]. Up to now, it is still a pendent imperative to further improve the subwavelength sound absorption performance of materials or structures.

With the in-depth study of sound absorption behavior, for one thing, more efficient sound-absorbing materials have been developed and confirmed as good candidates, including various carbon structures, aerogels, and composite fillers [21-23]. For another, from the aspect of structural acoustics, conventional microperforated plates, sandwich composite structures, and acoustic black hole (ABH) panels have been widely designed [24-26]. Furthermore, corresponding relationships were also systematically explored between geometric microstructure and acoustic properties. Especially, the Helmholtz resonator (HR) [27-29] has been used as one of the most acoustic structure models in engineering applications due to its simple, tunable, and durable characteristics. Based on the internal resonance effect principle, the combined sound absorption behaviors give the material good absorption performance of low-frequency sound waves, overcoming the drawbacks of traditional PMs. For instance, Wang et al. [29] proposed a sound-absorbing structure constructed by a microslotted plate and flexible perforated membrane. The higher sound absorption property was obtained in the high-bandwidth frequency and low-frequency domains by combining the Helmholtz effect with the microslit plate. Ren et al. [30] designed a hybrid structure consisting of midslits and microslits, and results showed that its sound absorption performance was excellent at

low and mid frequencies, even for a structure with a relatively thin thickness. Although these researchers practically and commercially demonstrated the effectiveness of novel structures in sound absorption, there are still obvious limitations, including controlling costs and ensuring that particular structures remain stable over long periods. Also, it is difficult to theoretically predict sound absorption characteristics since the composite structures have become more complex. The effect of composite structures on sound absorption characteristics has not been clarified yet in several cases.

The resonator structure significantly impacts a specific frequency in the mid-low-frequency range. However, the bandwidth of sound absorption is exceptionally narrow. To improve the sound absorption on low-frequency, in this chapter, the double cavity resonant device (DCRD) proposed in the chapter 2 is improved by using both porous materials (PMs) and microperforated panels (MPPs). Therefore, the sound absorbing performance is expected to be enhanced. With the above aim, herein, a double-cavity resonant device (DCRD) embedded with cambered PM and microperforated panel (MPP) was designed and fabricated based on the simplified HR model. First, two DCRD structures were prepared, and their sound absorption performances were measured and compared with two single cavity resonant devices (SCRD). Then, the sound absorption coefficient of each part was measured to clarify the contribution of parameters by the vertical incident approach. Finally, the sound absorption characteristics of DCRD were systematically discussed and compared with the classical Helmholtz resonance structure, especially in the low-frequency region. To sum up, we

proved that the proposed composite structure, DCRD, can be applied to broadband noise reduction with a smaller thickness. We hope it can provide a stepping stone for investigating the HR-based noise attenuation capacity and devices. For the same content of the air cavity, the sound absorption performance of the DCRD is twice higher as that of the HR structure. The developed DCRD could almost absorb low-frequency sounds without sacrificing high-frequency performance using the microperforated panel 3. The findings show that the optimization of noise reduction, especially for low-frequency sounds, is possible through a flexible design approach without increasing the structure's size.

The sound absorption characteristics of DCRD are discussed systematically and compared with the classical Helmholtz resonance structure, especially in the low-frequency region. We proved the proposed composite structure, a DCRD, could be applied to broadband noise reduction with a smaller thickness and hope it could provide a stepping stone for the investigation of the HR-based noise attenuation capacity and devices.

3.2 Experimental

3.2.1 Materials

Three porous materials (PMs) as shown in **Fig. 2-1**, including polyurethane wave foam (PUW, area density of 1.48 kg/m^2), polyurethane flat foam (PUF, area density of

1.43 kg/m^2) and glass wool flat foam (GWF, area density of 1.66 kg/m^2) are provided by supplied by FUJIFILM Wako Pure Chemical Corporation, Japan. The Helmholtz resonators' partition plate and the microperforated panels (MPPs) are made of medium-density fiberboard, and three types of MPPs are designed by changing their parameters, as listed in Table 2-4.

3.2.2 Configuration of the improved DCRD device

The double cavity resonant device (DCRD) was designed and prepared by assembling a nested structure with PMs and MPP (microperforated panel), as shown in **Fig. 3-1.** The MPP had a hole at the center for perforation and connection to the resonator. Both the MPP and the closed end of the duct end are rigid bodies. Briefly, the curved partition with a length of 15 mm and diameter of 80 mm is set at the neck of the Helmholtz so that the resonator can be naturally formed through the created space between the partition and the closed end and **Table 3-1**. The improved DCRD (sample 3), a double cavity resonant structure with PM inserted at the neck and MPP inserted inside is fabricated. **Fig. 3-2** shows four structures designed in this study for comparison. The sound absorption coefficient and impedance are measured according to standards of ISO 10534-1 and ISO 10534-2, which can be used to evaluate the sound absorption performance of materials (see Fig. 2-4).

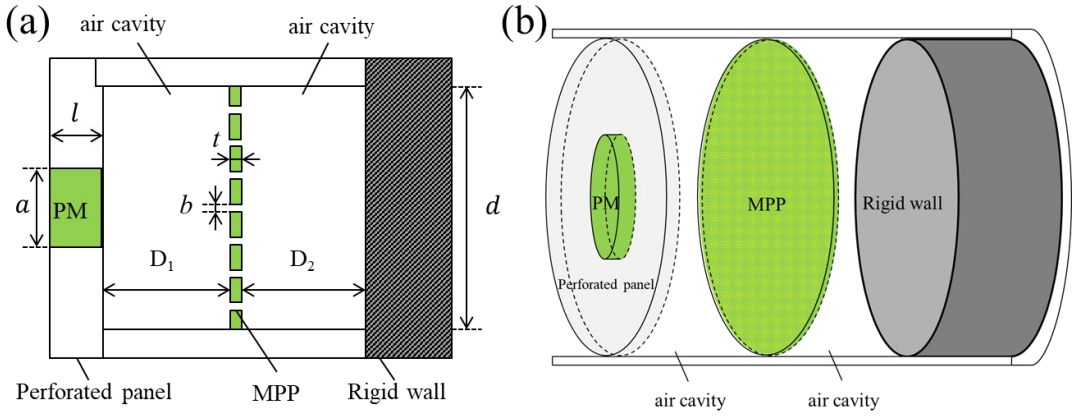

Fig. 3-1. 3D section viewing of the double cavity resonant device (DCRD).

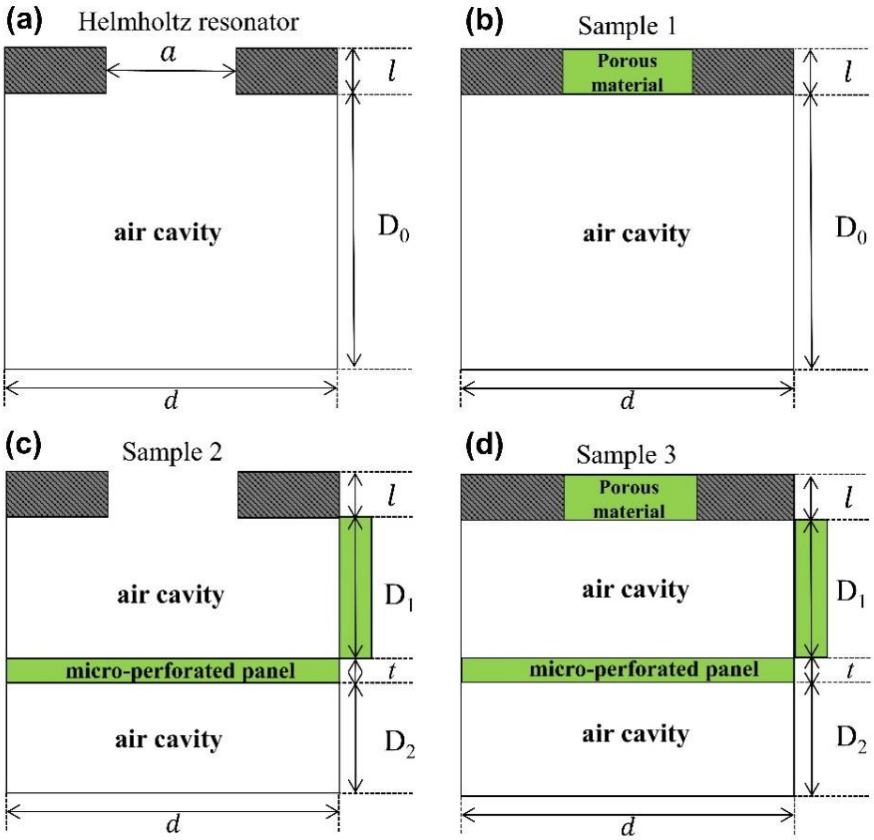

Fig. 3-2. Configurations of (a–b): single cavity resonant device (SCRD) and (c–d): DCRD.

3.2.3 Prediction absorption coefficients of the improved DCRD

The improved DCRD's total acoustic impedance is expressed as [31]

$$Z_t = Z_{tr} + iZ_{ti} = [Z_{MDF}^{-1} + Z_P^{-1} + Z_{MPP}^{-1} + Z_{DAC}^{-1}]^{-1} \quad (3\text{-}1)$$

where Z_{MDF}, Z_P, Z_{MPP}, and Z_{DAC} represent the acoustic impedances of MDF, porous, MPP, and the double air cavity inserted in HR, respectively. The MDF's acoustic impedance was predicted through wave propagation in MDF, as $Z_{MDF} = Z_c \coth(ik_{MDF}l/\rho_0 c_0)$, where ρ_0 represents the density and c_0 represents the wave speed of air. The characteristic impedance, Z_c and wavenumber, k_{MDF} of the MDF were obtained as $Z_c = (\rho_{MDF} K_{MDF})^{0.5}$ and $k_{MDF} = \omega(\rho_{MDF}/K_{MDF})^{0.5}$, respectively. The effective density, ρ_{MDF} and bulk modulus, K_{MDF}, were given as [32]

$$\rho_{MDF} = \rho_0\left[1 + (\delta/a)\sqrt{2/i}\right] \quad (3\text{-}2)$$

$$K_{MDF} = \frac{\gamma P_0}{\gamma - (\gamma - 1)/1 + (\delta/Ba)\sqrt{2/i}} \quad (3\text{-}3)$$

where γ, B, P_0, and a represent the specific heat ratio, square root of the Prandtl number, atmospheric pressure, and slit thickness, respectively. $\delta = (2\eta/\omega\rho_0)^{0.5}$ is the viscous skin depth, where η represents the shear viscosity.

The acoustic impedance of the PM inserted $Z_P = Z_c coth\gamma l$. The characteristic impedance, Z_c, and specific acoustic resistance, γ, of the porous was obtained as $Z_c = R + jX$ and $\gamma = \alpha + j\beta$, respectively, which were given as [33]

$$Z_c = 1 + 0.070\left(\frac{f}{R}\right)^{-0.632} + i\,0.107\left(\frac{f}{R}\right)^{-0.632} \tag{3-4}$$

$$\gamma = k\left\{0.160\left(\frac{f}{R}\right)^{-0.618}\right\} + ik\left\{1 + 0.109\left(\frac{f}{R}\right)^{-0.618}\right\} \tag{3-5}$$

where $R\ and\ \alpha$ represent the specific acoustic resistance and the absorption coefficient of the porous.

The acoustic impedance of the MPP inserted $Z_{MPP} = r + j\omega m,$ the normalized specific acoustic resistance of r and ωm were given as [34]

$$r = \frac{32\eta t}{p\rho_0 c_0 d^2}\left(\sqrt{1 + \frac{k^2}{32}} + \frac{\sqrt{2}}{32}k\frac{d}{t}\right) \tag{3-6}$$

$$\omega m = \frac{\omega t}{pc_0}\left(1 + \frac{1}{\sqrt{9 + \frac{k^2}{2}}} + 0.85\frac{d}{t}\right) \tag{3-7}$$

$$k = d\sqrt{\frac{\omega\rho_0}{4\eta}} \tag{3-8}$$

where ρ_0, $c_0, t, d,$ and p represent the density of air, the sound velocity in air, the thickness (mm), the aperture diameter (mm), and the aperture ratio of MPP, respectively.

The acoustic impedance of the double air cavity inserted $Z_{DAC} = [Z_{PAC}^{-1} + Z_{MAC}^{-1}]^{-1}$. D_1 represents the depth of the air cavity between PM and MMP, D_2 represents the depth of the air cavity between MPP and rigid wall. The acoustic impedance,Z_{PAC}, Z_{MAC}, of the air space were obtained as $Z_{PAC} = icotkD_1$ and $Z_{MAC} = icotkD_2$, respectively. The predicted sound absorption coefficient α for the DCRD was expressed as follows，

$$\alpha = \frac{4Z_{tr}}{(1+Z_{tr})^2 + Z_{ti}^2} \tag{3-9}$$

3.3 Results and discussions

3.3.1 The effect of the PMs on the sound performance of DCRD

We assembled MPP into SCRD to obtain DCRD and characterized the sound absorption performance. The measured acoustic curves are illustrated in **Fig. 3-3, 3-4, 3-5** and it can be found that the curves have a dramatic variation compared with that of SCRD **(**see **Fig.2-6)**.

To investigate the effect of PMs on the DCRD's acoustic performance, the PMs, PUF, and GWF were used, and the cavity size was fixed. Multiple peaks with a relatively high sound absorption coefficient appeared on the measured acoustic properties of Sample 3. Peaks 1, 2, and 3 from the low-frequency side, the maximum sound absorption coefficient and the frequency behaviour. The sound absorption coefficient at Peak 1 of 321 Hz for Sample 3_GWF_MPP3_D16 was 1.42 times that of Sample 3_GWF_MPP1_D16. At Peak 2, the peak sound absorption coefficient was shown near 450 Hz even when the MPP area ratio changed, and Sample 3_GWF_3_D16 exhibited the highest sound absorption coefficient of 0.79. However, at Peak 3, the frequency shifts to a relatively high-frequency with a big frequency change, and the absorption also changes visibly. Table 5 shows the detailed acoustic characteristics of the DCRD with both PM and MPP design changes. Thus, the acoustic performance tends to be a combination of the MPP design and PMs. The holes in MPP and the porous structures in PMs contribute to the absorption coefficients. The friction's absorption effect increased with the number of holes. The incident, reflection and sound absorption were repeated in holes and also absorbed by reflection from one hole to another. The amount of absorption energy increased, eventually, may also be considered as the volume of air in the DCRD increased. The sound absorption mechanism of the DCRD depends on the structure of the porous sound absorber, Helmholtz resonator, and MPP design, and the multi-frequency peaks appear due to their combined effect. The MPPs appeared to have higher absorption performance than the Helmholtz resonator. The absorption performance of different area ratios had a massive effect on the resonance frequency

and peak frequency changes. Regarding PMs, the sound absorption coefficient varies depending on the fiber diameter and moulding conditions, even if the density is the same. For this reason, flow resistance is a better quality specification for PMs than density [35].

3.3.2 The effect of the MPPs on the sound performance of DCRD

As another important component used in the assembly of DCRD, the acoustic performance of MPPs is also crucial. In this section, single MPPs and sound absorption coefficient were taken as research objects and optimization targets. Also, systematical exploration was carried out to investigate the area ratio influence, a key parameter, and determine a good option. Three samples with different area ratios (from 40% to 160%) were prepared, named MPP1, MPP2, and MPP3, as shown in **Table 2-1**. The sound absorption coefficient of three MPP samples combined with different area ratios at different cavity depths (D_2) from 4 mm to 50 mm was investigated systematically in our previous paper [36-40].

The DCRD (Sample 3) was further prepared by using MPPs (area ratio of 0.4, 0.8 and 1.6) and PMs (PUW, PUF and GWF), and the effect of MPPs on sound absorption performance is evaluated. The results are shown in **Fig. 3-3, 3-4 and 3-5**.

In general, the introduction of PMs enables DCRD samples assembled by MPPs with a low area ratio (0.4) to produce sound-absorption coefficient peaks for the sound wave in the low-frequency region, which makes up for the poor sensitivity of SCRD to low-

frequency acoustic wave energy and reflects the advantages of the double-cavity device. However, the peak position and intensity almost remain unchanged, and the same peak shift phenomenon can also be observed. On the other hand, as mentioned above, because the sound-absorbing energy of PUF is significantly stronger than GWF, the DCRD map shows a higher sound-absorbing coefficient peak for PUF-embedded samples with the same test parameters. Also, another key point that needs to be noted is that there is an obvious positive correlation between the cavity depth and the sound-absorption coefficient of the curve from whole **Fig. 3-3, 3-4 and 3-5**. However, when the depth value is large, the gain of the sound-absorption coefficient is no longer evident. Taking a typical peak of 420Hz as an example, 0.92 seems to reach a peak point.

To improve DCRD (Sample.3) was prepared by using MPPs (area ratio of 0.4, 0.8 and 1.6) and PMs (PUW, PUF and GWF), and the effect of depth on sound absorption performance was evaluated. The results are shown in **Fig. 3-3, 3-4 and 3-5**.

For the sound absorption coefficient of flat foam different hole shape the introduction of PMs enables DCRD samples assembled by MPPs with a low area ratio (0.4) to produce sound-absorption coefficient peaks for the sound wave in the low-frequency region, which makes up for the poor sensitivity of SCRD to low-frequency acoustic wave energy and reflects the advantages of the double-cavity device. However, the peak position and intensity almost remain unchanged, and the same peak shift phenomenon can also be observed. It can be found that the curves have a dramatic variation compared with that of SCRD. In detail, due to the existence of double-cavity resonator structure, three typical peaks were observed at 220 Hz, 420 Hz, and 725 Hz approximately for

both two PMs. And from the perspective of the intensity for sound-absorption coefficient when samples possess the same cavity volume (with the same D value of 36 mm), the PUF sample also has a slight advantage and shows a maximum value of 0.92 (0.8 of PUW) attribute to the improvements of the frictional effect for the internal air. Since air vibrations exist in the DCRD air cavity, the higher resonance frequency usually means improved sound absorption performance, indicating that the weak sound absorption performance of pure PMs can be further improved by proper structure design.

3.3.2 The effect of the air distance on the sound performance of DCRD

On the basis of fixed cavity size (16 mm of D_1, 15 mm of D_2), we embedded the PUF and GWF mentioned above as typical PMs models to generate a complete DCRD, and systematically studied the comprehensive influence of PMs and MPPs on the acoustic performance of this DCRD. Sample 3 (MPP3) was chosen as an optimization target, and the acoustic curves are tested. It can be found that after assembling the full DCRD structure, compared with the simple cavity resonator, the acoustic curve of DCRD shows multiple peaks of sound absorption coefficient in the frequency range of 170-950 Hz, and the corresponding sound absorption coefficient shows a huge improvement. For the curves of PUW and PUF as PMs, typical characteristic peaks appear in the low-frequency, medium-frequency and high-frequency regions corresponding to 200-300 Hz, 400-500 Hz and 700-800 Hz, respectively. Moreover, the peaks value is close to each other with little change. All their highest peaks are also found at ~430 Hz, which

is about 0.97. However, the sound absorption curve of DCRD combined with PUW/PUF and MPP3 has a great variation compared with the former two. It is obvious that the characteristic peak in the high-frequency region disappears, and the characteristic peak in the low-frequency region shifts from ~220 Hz to ~330 Hz, and the value of sound absorption increases 1.42 times that of MPP1 and MPP2.

On the other hand, for the DCRD samples assembled by PUF samples, the distribution and variation law of the peaks of the sound-absorption coefficient is consistent with PUW in general, but for the sound-absorption coefficient representing the absorption value, PUF samples obviously show a better performance, which is consistent with the previous test results. Overall, it can be seen that the acoustic performance is the result of the synergistic effect of MPPs and PMs. Thus, the multi-frequency peaks appear due to their combined effect and are closely related to the properties and structure distribution of the two. For our DCRD system, the sound absorption mechanism depends on the PMs structure, Helmholtz resonator and MPP design. The holes in MPPs and the porous structure in PMs are significant contributions to the absorption coefficient. The absorption effect of friction in holes also increases with the increase of the holes. The whole process of sound absorption results from the incident's joint action, reflection of the sound wave. In these physical processes, the sound wave eventually disappears with the conversion of energy into internal energy.

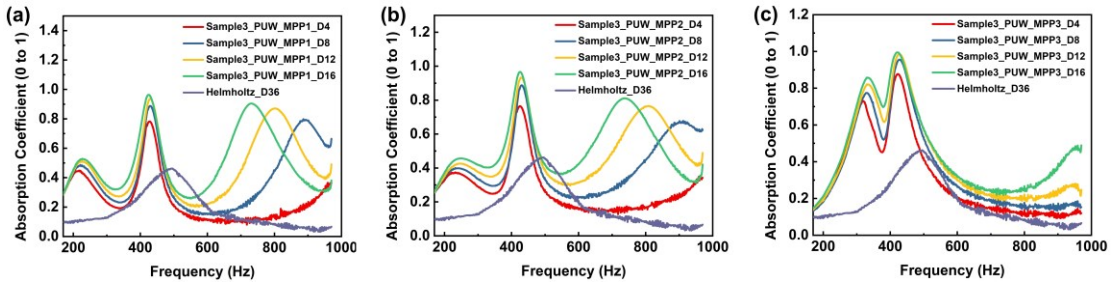

Fig. 3-3. Measured absorption coefficients of Sample 3_PUW (DCRD), the area ratio of MPP = (a) 0.4, (b) 0.8, (c) 1.6. The surface densities of PUW = 1.48 kg/m^2, the depth of the Helmholtz resonator = 36 mm, the air cavity depth 4 mm ≦ D1 ≦ 16 mm, and other design parameters were kept constant for the tested samples.

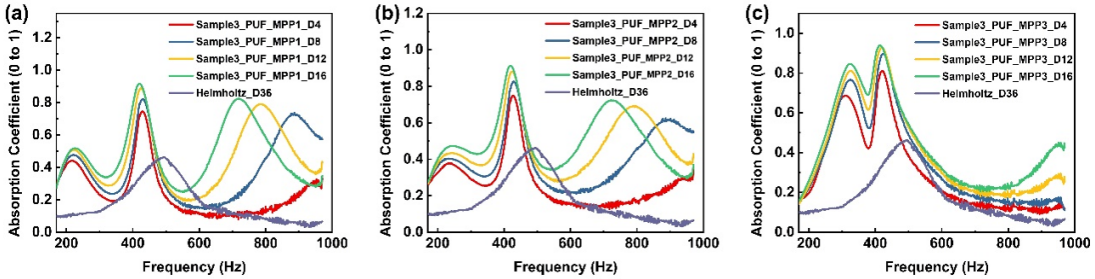

Fig. 3-4. Measured absorption coefficients of Sample 3_PUF (DCRD), the area ratio of MPP = (a) 0.4, (b) 0.8, (c) 1.6. The surface densities of PUW = 1.48 kg/m^2, the depth of the Helmholtz resonator = 36 mm, the air cavity depth 4 mm ≦ D1 ≦ 16 mm, and other design parameters were kept constant for the tested samples.

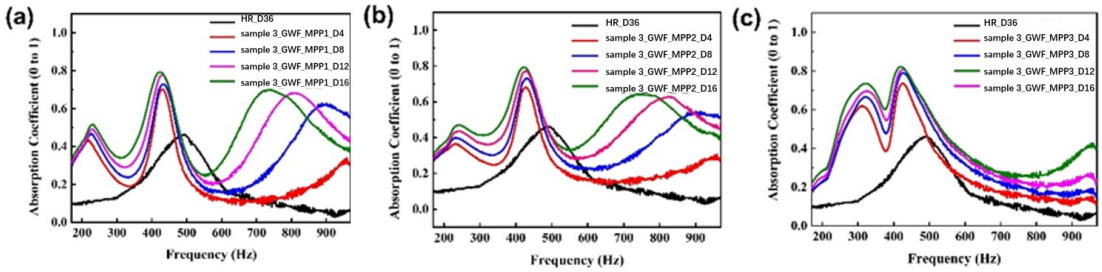

Fig. 3-5. Measured absorption coefficients of Sample 3_GWF (DCRD), the area ratio of MPP = (a) 0.4, (b) 0.8, (c) 1.6. The surface densities of GWF = 1.66 kg/m2, the depth

of the Helmholtz resonator = 36 mm, the air cavity depth 4 mm ≦ D1 ≦ 16 mm, and other design parameters were kept constant for the tested samples.

3.4 Conclusion

To sum up, in this work, the DCRD with multi-band sound absorption characteristics was proposed. In order to form this novel structure with two air cavities for sound absorption, we do a necessary structural improvement to the traditional Helmholtz resonator, and the key point is the insertion of sound-absorbing PMs in the neck of the DCRD and MPPs inside the resonator, respectively. Then, the sound absorption coefficient and the peak frequency of sound absorption are investigated by systematic experiments. This work did not intend to chemically modify the porous sound-absorbing materials, but to force the sound energy at different frequencies to be concentrated and distributed in multiple regions through the designed composite, and then be absorbed and dissipated. And the results reveal that the sound absorption performance of DCRD is more than 200% higher than that of the Helmholtz resonance structure. And developed DCRD could almost absorb low-frequency sounds without sacrificing high-frequency performance with the insertion of MPPs. We believe this result can be applied to the design of composite sound-absorbing porous materials and possesses potential applications in architectural acoustics product design and industrial equipment vibration for noise reduction.

By comparing the two PMs, GWF and polyhedrane foams show good absorption performance, while polyurethane may be better for use as an inserting PM. The design parameters, such as the surface density of PMs, the air cavity's depth, and the area ratio of MPP, will have a combined effect on the resulting sound performance, which is controllable and could be optimized. Therefore, the DCRD structures may offer a new tool for multi-band sound absorption design, especially for low-frequency sound absorption fields. The absorption effect of SCRD/DCRD with wave foam is better than that of flat foam. Furthermore, the continuous round hole shape is better than slit holes.

Reference

[1] M. Yang, P. Sheng, *Annu Rev Mater Res*, **247**, 83-114 (2017).

[2] D. Wang, L. Ying, Y. Jia, L. Zhang, F. Zhang, W. Wang, *J Clean Prod*, **245**, 118911 (2020).

[3] K. Persson, M. Smith, L. Hussain-Alkhateeb, A. Koopman, M. Ögren, E. Peris, W. David, J. Woodcock, C. Sharp, *Environ. Polluti.,* **245**, 558-67 (2019).

[4] Y. Fu, *ChemistrySelect*, **17**, e202103222 (2022).

[5] L . Wang, F-S. Zhang, *Constr Build Mater*, **157**, 237-43 (2017).

[6] X. Zhang, Z. Qu, H. Wang, *IScience*, **23**, 101110 (2020).

[7] M. Yang, S. Chen, C. Fu, P. Sheng, *Mater Horiz*, **4**, 673-680 (2017).

[8] Y.I. Bobrovnitskill, T.M. Tomilina, *Acoust Phys*, **64**, 519-526 (2018).

[9] L. Cao, Q. Fu, Y. Si, B. Ding, J. Yu, *Compos Commun*, **10**, 25-35 (2018).

[10] S. Amares, E. Sujatmika, T. Hong, R. Durairaj, H. Hamid, *J Phys: Conf Ser*, **908**, 012005 (2017).

[11] T. Ulrich, J. Arenas, *Sustainability*, **12**, 2361 (2020), 243, 569-678 (2001).

[12] N. Atalla, R. Panneton, F.C. Sgard, X. Olny, J. Sound Vib,

[13] S. Ersoy, H. Küçük, *Appl Acoust*, **70**, 215-220 (2009).

[14] W. Yang, Y. Li, *Sci China Technol Sc*, **55**, 2278-2283 (2012).

[15] M. Liang, H. Wu, J. Liu, Y. Shen, G. Wu, *J Porous Mater*, **29**, 869-92 (2022).

[16] D. Zong, L. Cao, X. Yin, Y. Si, S. Zhang, J. Yu, B. Ding, *Nat Commun*, **12**, 6599 (2021).

[17] R. Dunne, D. Desai, R. Sadiku, *Acoust Aust*, **45**, 453-69 (2017).

[18] S. Selvaraj, V. Jeevan, R-R. Jonnalagadda, N-N. Fathima, *J Clean Prod*, **213**, 375-83 (2019).

[19] B-S. Kim, J. Park, *Compos. Struct*, **183**, 545-9 (2018).

[20] L. Chang, A. Jiang, M. Rao, F. Ma, H. Huang, Z. Zhu, Y. Zhang, Y. Wu, B. Li, Y. Hu, *RSC Adv*, **11**, 37784-800 (2021).

[21] Y. Wu, X. Sun, W. Wu, X. Liu, X. Lin, X. Shen, Z. Wang, R. Li, Z. Yang, K. Lau, J. Kim, *Compos Part A-Appl S*, **102**, 391-399 (2017).

[22] Y-j. Qian, D-Y. Kong, Y. Liu, S-M. Liu, Z-B. Li, D-S. Shao, S-M. Sun, *Appl Acoust*, **82**, 23-27 (2014).

[23] K-W. Oh, D-K. Kim, S-H. Kim, *Fibers Polym*, **10**, 731-737 (2009).

[24] N. Gao, J. Wu, K. Lu, H. Zhong, *Mech Syst Signal Pr*, **154**, 107504 (2021).

[25] W. Chen, T. Chen, F. Xin, X. Wang, X. Du, T-J. Lu, *Mater Design*, **105**, 386-97 (2016).

[26] Y. Tang, F. Li, F. Xin, T-J. Lu, *Mater Design*, **134**, 502-12 (2017).

[27] Y. Tang, S. Ren, H. Meng, F. Xin, L. Huang, T. Chen,C. Zhang, T. Lu, *Sci Rep*, **7**, 43340 (2017).

[28] D. Jun, O. Nespesny, J. Pencik, Z. Fisarova, A. Rubina, *Appl Acoust*, **184**, 108341 (2021).

[29] Y. Wang, C. Zhang, L. Ren, M. Ichchou, M-A. Galland, O. Bareille, *Compos Struct*, **108**, 400-408 (2014).

[30] S-W. Ren, H. Meng, F-X. Xin, T-J. Lu, Chinese Phys Lett, 32, 014302 (2015).

[31] Standard ISO 10534-1, Acoustics－ Determination of sound absorption coefficient and impedance in impedance tubes Part 1 (1998).

[32] Standard ISO 10534-2, Acoustics－Determination of sound absorption coefficient and impedance in impedance tubes Part 2 (1998).

[33] Standard ASTM E1050-98, Standard test method for impedance and absorption of acoustical materials using a tube, two microphones and a digital frequency analysis system (1998).

[34] M. Koyasu, *Arch Acoust. noise control*, **19**,71 (1990).

[35] M. Koyasu, *Arch Acoust. noise control*, **15**, 54 (1986).

[36] Dah-You Maa, *Scientia Sinica*, **18**, 55-71 (1975).

[37] Dah-You Maa, *Noise Control*, **29**, 77-84 (1987).

[38] Dah-You Maa, *J Acoust Soc Am*, **104**, 2861 (1998).

[39] Dah-You Maa, *Int J Acoust Vib*, **12**, 3-6 (2007).

[40] W. Yang , H. Xia, Q-Q. Ni, *Appl Acoustic*, 206, 109304 (2023).

Chapter 4: Design and properties of the laminated sound-absorbing materials using natural straw and rice husk

4.1 Introduction

Many materials used as sound-absorbing materials are porous materials [1-7]. Porous materials have sound absorption characteristics, such as excellent sound absorption performance in high-frequency bands [8-12]. As a result, noise in the mid-to-low-frequency range, such as the sound of conversations and cars running on the road, has become a problem [13-16]. In addition, from the global environmental protection viewpoint, attention is also focused on materials that make up sound-absorbing materials. This is because it will lead to society's realization and a recycling-based society [17-20]. In addition, depending on the location where they are used, the added value required for sound-absorbing materials changes. There are many demands for sound-absorbing materials, but in any case, it is required to develop sound-absorbing materials that meet the needs of the times [21-24].

Sound-absorbing materials and mechanisms are generally broadly classified into the following three categories [25-28]: (i) Porous type sound absorption, composed of materials with many pores, fiber materials (glass wool, rock wool, non-woven fabric, etc.) and foam materials (urethane foam, etc.). The sound absorption performance of these materials is small in the low-frequency range and large in the high-frequency range. (ii) Plate vibration type sound absorption, including plate-like materials such as gypsum board, plywood, and metal plate. And (iii) biomass materials, consisting of

natural waste materials [29-31]. Many porous biomass materials have been developed for sound absorption. Rice straws and rice husks have shown high sound absorption performance and are helpful as sound-absorbing materials.

In this work, we constructed a multi-layer sound-absorbing structure made of natural materials by laminating it with a perforated Medium Density Fiberboard (MDF) and evaluated its sound-absorbing properties. Generally, a multi-layered sound-absorbing structure consisting of perforated plates and porous materials is effective for sound absorption in the middle-frequency range [32-33]. Gypsum board is often used as the perforated plate, and glass wool or non-woven fabric is often used as the porous material. Here we developed a sound-absorbing structure using MDF and a sound-absorbing material made of rice straw and rice hulls and clarified the influence of the related parameters on the sound-absorbing performance. This led to a more accurate understanding of the measurement results with natural materials.

4.2 Experimental

4.2.1 Materials

Natural rice straw and rice husks were used as raw materials to fabricate the composite sound absorption materials. Its internal structures with various gaps were moderately small and quickly generated the viscous resistance of the air when the acoustic wave was incident. Thus, a favourable sound-absorbing effect could be expected.

4.2.2 Preparation of composite sound absorption structure based on rice straw

Commercially available garden straw was cut into 20 mm lengths as shown in **Fig. 4-1(a)** and classified by diameter as shown in **Fig. 4-1(a) (ii)** and **(iii)**. In this study, the straws with a diameter of 3 mm or more are treated as thick straw, and the straws with a diameter of less than 3 mm are treated as thin straw. By combining with the rice husk **Fig. 4-1(a) (iv),** a sound-absorbing material is fabricated. Height, diameter (width), and average mass are shown in **Table 4-1**.

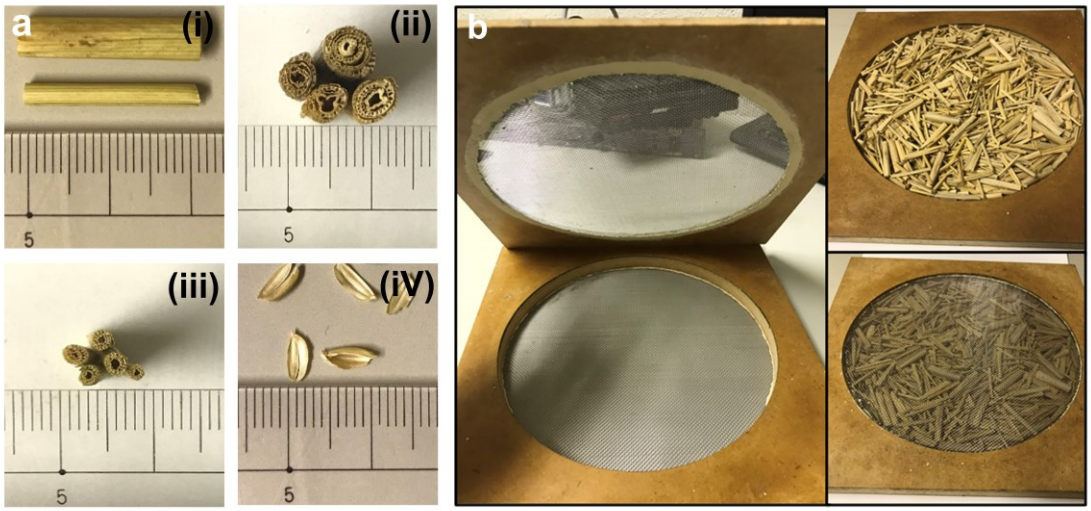

Fig. 4-1. (a) Digital images of straw (20 mm). (b) Method of molding Rice straw as a porous material.

Table 4-1. Dimensions and weight of Rice straw element and Rice husks element.

	Length [mm]	Diameter (width) [mm]	Average weight per one piece [mg]
Thick rice straw element	20	3 - 6	59
Thin rice straw element	20	1 – 2.9	15
Rice husks element	5 - 7	2 - 3	1.6

In order to treat materials such as rice straw and rice husks, which have variations in shape, as porous sound-absorbing materials, we must use an unique method to pour them into a frame and fill in them and then mold them into a fixed shape with an adhesive or the like (**Fig. 4-1b)**. A wooden frame was prepared and a hole of the same size as the inner diameter of the acoustic tube was drilled in the wooden frame. The rice straw and rice husks were formed into a certain shape by this method. In addition, the wire mesh was attached so that the surface of the wooden frame was not uneven, and it was confirmed that it did not affect the acoustics.

4.2.3 Normal incident sound absorption coefficient test

An acoustic tube was used for the normal incidence sound absorption coefficient. There were two types of acoustic tubes, thick and narrow, depending on the tube size. The measurable frequency band was in the middle-frequency band to measure the specimens with inhomogeneous structures and perforated plates.

The normal incidence sound absorption coefficient test was conducted to determine the sound absorption coefficient. The outline is shown in Figure 2 and summarized below. A full-range loudspeaker 20F-20 (Technics), two condenser microphones ISOMAX (COUNTRYMAN), and audio interface Fireface400 (RME) were used for signal generating, sound pressure-field measuring, and signal processing. A noise sound was generated from the speaker of the tube, and each sound waveform was measured with two microphones attached to the side of the tube [6]. The sound absorption coefficient and impedance were measured according to standards of ISO 10534-1 [34] and ISO 10534-2 [35], which can be used to evaluate the sound absorption performance of materials. For normal sound incidence, an impedance tube, two microphone locations, and a digital frequency analysis system were employed to measure the sound absorption coefficient of sound absorbers. Before the testing, the sound-absorbing tube should be put straight, and the inside surface should be smooth, nonporous, and dust-free to ensure effective sound attenuation [36].

For measuring the specimens with inhomogeneous structures and perforated plates, and the measurable frequency band is in the middle frequency band, It is suitable to use the thick acoustic tube self-made as shown in **Fig. 4-2a**. A loudspeaker is installed at one end, a rigid wall is installed at the other end, and two microphones are installed on the side. The test piece is placed so that it is sandwiched between the rigid wall and the pipe end. The normal incidence sound absorption coefficient test is conducted to determine the sound absorption coefficient. The outline is as shown in **Fig. 4-2b** and summarized below. A noise sound is generated from the speaker of the tube, and each

sound waveform is measured with two microphones attached to the side of the tube. Then, the complex transfer function between the two microphones is obtained, and the complex sound pressure reflectance is calculated. From this, the normal incidence sound absorption coefficient is obtained.

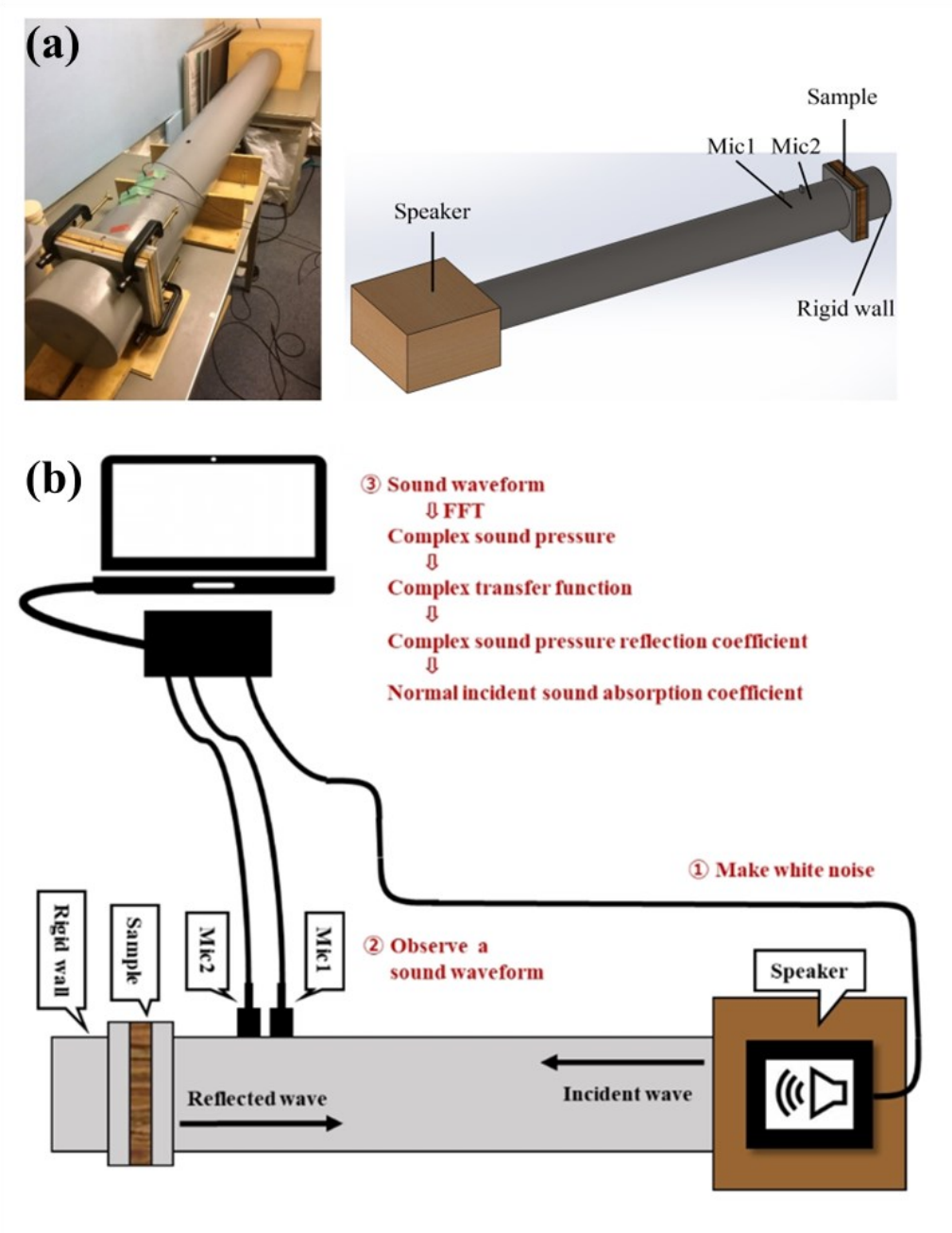

Fig. 4-2. Experiment procedure of sound absorption coefficient.

4.2.4 Measurement of sound absorption coefficients

Acoustic characteristics of the multi-layer structures are usually analyzed by the transfer matrix method in the frequency region where the plane wave theory is efficient. In this method, the precise estimation of the transfer matrix is important. The propagation constant, the acoustic impedance and the transfer matrix of any duct element are required, which can precisely predict the acoustic characteristics of a total duct system. The sound absorption coefficient, α, can be calculated by the transfer matrix method using Eq. (1–3), if the sound, I_i, is the incident wave and I_r is the reflected wave, where s represents the distance between microphone 1 and microphone 2, $H_{12} = P_2 \,/\, P_1$ represents the two microphone signals' transfer function corrected for microphone response mismatch, and r represents the reflection coefficient [37]. Then, the normal incidence sound absorption coefficient was obtained.

$$\alpha = 1 - \frac{I_r}{I_i} \tag{4-1}$$

$$r = \frac{H_{12} - e^{-jk_0 s}}{e^{jk_0 s} - H_{12}} e^{2jk_0 x_1} \tag{4-2}$$

$$\alpha = 1 - |r|^2 \tag{4-3}$$

The predicted acoustic impedance in this study is expressed as [38]

$$\mathrm{Z}_t = Z_{tr} + iZ_{ti} = [Z_{Material}^{-1} + Z_{Air}^{-1}]^{-1} \tag{4-4}$$

where the Z_M, Z_A are the acoustic impedances of porous material and air cavity, respectively. The acoustic impedance was calculated through wave propagation, as $Z_M = Z_c \coth(ik_M l/\rho_0 c_0)$, where ρ_0 represents the density and c_0 represents the wave speed of air. The characteristic impedance, Z_c and wavenumber, k_M of the material were obtained as $Z_c = (\rho_M K_M)^{0.5}$ and $k_M = \omega(\rho_M/K_M)^{0.5}$, respectively. The effective density, ρ_M and bulk modulus, K_M, were given as [39]

$$\rho_M = \rho_0\left[1 + (\delta/a)\sqrt{2/i}\right] \tag{4-5}$$

$$K_M = \frac{\gamma P_0}{\gamma - (\gamma - 1)/1 + (\delta/Ba)\sqrt{2/i}} \tag{4-6}$$

where γ, B, P_0, and a represent the specific heat ratio, square root of the Prandtl number, atmospheric pressure, and slit thickness, respectively. $\delta = (2\eta/\omega\rho_0)^{0.5}$ is the viscous skin depth, where η represents the shear viscosity.

The acoustic impedance of the air cavity Z_A. D_0 represents the air cavity depth between the material and the ridge wall. The acoustic impedance,Z_A, of the air space were obtained as $Z_A = icotkD_0$. The predicted sound absorption coefficient α was expressed as follows，

$$\alpha = \frac{4Z_{tr}}{(1 + Z_{tr})^2 + Z_{ti}^2} \tag{4-7}$$

4.3 Results and discussions

4.3.1 Sound absorption properties of different rice straw

Thick and thin rice straws were used to compare the sound absorption characteristics depending on the thickness of the straw. Three samples were prepared: a sample filled with thin straw and a sample filled with a mixture of thick and thin straws shown in **Fig. 4-3(a-c)**. **Table 4-2** shows the mass and bulk density of the sample. The thickness of each sample is 15 mm.

Fig. 4-3. (a) Thick rice straw. (b) Thin rice straw. (c) Thick rice straw + Thin rice straw.

Table 4-2. Weight and bulk density of Rice straw absorber.

	Weight [g]	Bulk density [kg/m³]
Thick rice straw	46.2	98.1
Thin rice straw	55.5	117.8
Thick rice straw + Thin rice straw	50.9	108.0

Fig. 4-4 (a-c) show the sound absorption coefficients of the samples with 0 mm, 15 mm and 30 mm of air layer behind them, respectively. For all samples, the sound absorption coefficient seems monotonous increase in the frequency region of less than 900 Hz. When the air layer becomes large, the slope of monotonous increment increased. The sound absorption coefficients of the samples with thin straw and those with a mixture of thick and thin straw were comparable, while the thick straw sample showed slightly better sound absorption than the others in the frequency band above 600 Hz. This is considered to be due to the fact that the thicker straw has a larger exposed cross-section and sound waves tend to enter the fine gaps in the rice straw cross-section. In addition, the thick straw sample has the lowest bulk density, making it the most useful sound-absorbing material in terms of its light weight. The other acoustic characteristics, impedance, damping constant, and phase velocity are shown in supporting information in **Fig. 4-5(a-c)**. In the characteristic impedance (solid part), the thick and thin straw samples had linear graphs, while the thick and thin straw mixture

sample had a slightly undulating graph. This indicates that the internal structure of the sample has become more complex due to the mixture of thick and thin straws. In terms of phase velocity, the smallest value means that more resistance is encountered in the propagation of sound, such as stagnation in the solid part of most sound-energy materials, and more vibrations are generated, lost, and consumed by the interaction. The thick straw sample showed the smallest value in the entire frequency range. This reflects that the impedance in the material was the largest.

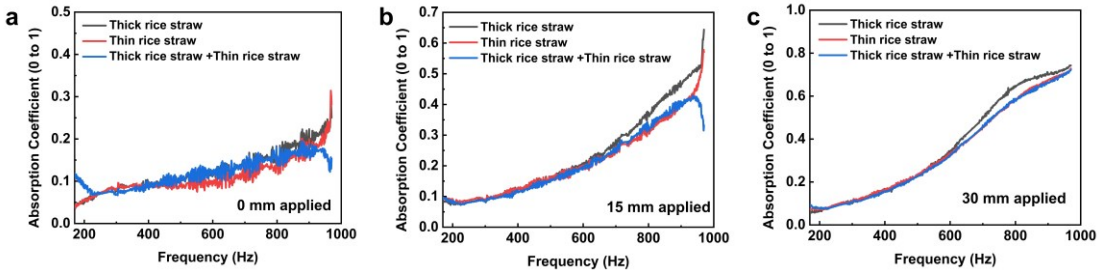

Fig. 4-4. Sound absorption coefficient of Rice straw absorber with different air cavity.

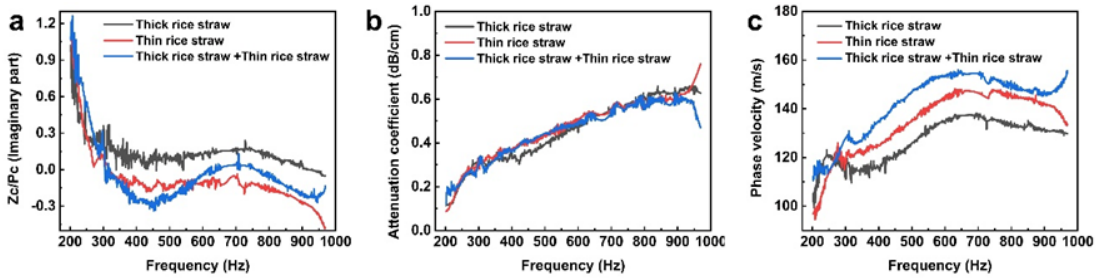

Fig. 4-5. (a) *Zc/ρc* of the rice straw absorber. (Compared with rice straw diameter). (b) The attenuation coefficient of the rice straw absorber. (c) The phase velocity of the rice straw absorber.

4.3.2 Sound absorption properties of rice straw mixed with rice husk

Using thick rice straw and rice husks, the change in sound absorption characteristics when rice straw is mixed with rice husks was clarified. Two new samples were prepared, one filled with rice husk shown in **Fig. 4-6a** and the other filled with a mixture of thick rice straw and rice husk shown in **Fig. 4-6b**, and the sound absorption coefficient, characteristic impedance, attenuation constant, and phase velocity were measured. The thickness of both samples is 15 mm. **Table 4-3** shows the mass and bulk density of the sample.

Fig. 4-6. (a) Rice husks absorber. (b) Absorber mixed with tick rice straw and rice husks.

Table 4-3. Weight and bulk density of Rice straw and Rice husks absorber.

	Weight [g]	Bulk density [kg/m³]
Rice husks	63.5	134.8
Thick rice straw +Rice husks	64.7	137.4

Fig. 4-7 (a-c) show the sound absorption coefficient of each sample when the back air layer is 0 mm, 15 mm, and 30 mm. The sound absorption coefficient was shown, and it was found that the sound absorption coefficient was sufficiently practical. This is thought to be due to the fact that the gaps between the rice straws formed when the rice straws are filled become finer due to the inclusion of rice husks, making it easier for viscous resistance to occur in the air.

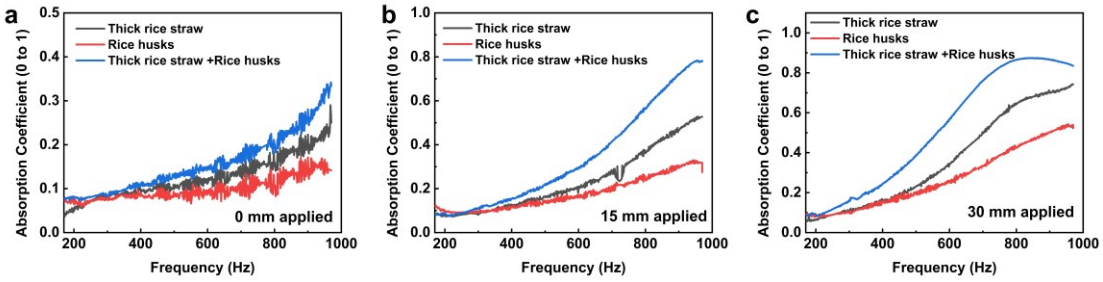

Fig. 4-7. Sound absorption coefficient of Rice straw and Rice husks absorber with different air cavity.

Fig. 4-8 (a-c) show the characteristic impedance, damping constant, and phase velocity of each sample. This indicates that the sound waves in the material are difficult to move. The attenuation constant also showed the largest value. This indicates that the

attenuation of the sound waves in the material is large. The velocity showed the smallest value, which means that the sound velocity in the material is slow. On the other hand, focusing on the rice husk, the characteristic impedance (real part) showed the smallest value and the phase velocity showed the largest value. This indicates that the speed of sound is high, and it is thought that the rice husk sample showed the highest sound absorption coefficient.

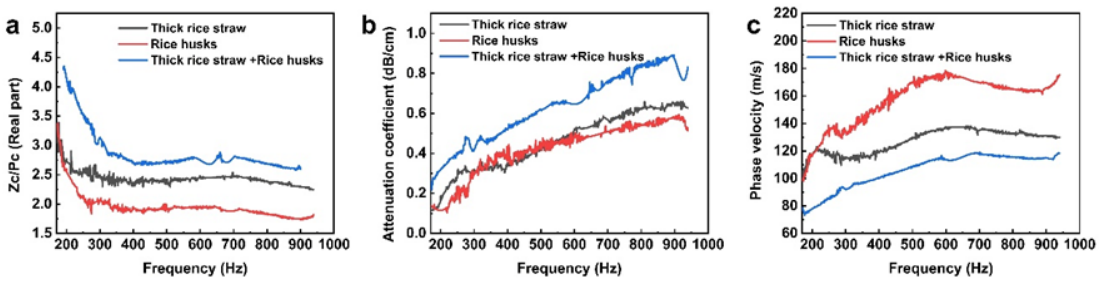

Fig. 4-8. (a) *Zc/pc* of the rice straw and rice husk absorber (Effect of mixing rice husks). (b) The attenuation coefficient of the rice straw and rice husk absorber. (c) The phase velocity of the rice straw and rice husk absorber.

4.3.3 Sound absorption properties of samples filled with a mixture of thick rice straw and rice husks

Regarding the sample filled with a mixture of thick rice straw and rice hulls, which showed the best sound absorption performance so far, the nonwoven fabric (Tokyo Soundproof Co., Ltd., product name: White Kyuon) shown in **Fig. 9a** and the nonwoven fabric shown in **Fig. 9b**. We compared the sound absorption characteristics with the sample filled with rice straws and rice husks prepared in our previous research. The rice

straw element of the sample mixed with husks was 15 mm in length, and both thick and thin straws were mixed without thickness distinction. **Table 4-4** shows the mass and bulk density of the sample for comparison.

Table 4-4. Weight and bulk density of comparison sample.

	Weight [g]	Bulk density [kg/m³]
Non-woven	13	27.6
Thick rice straw + Rice husks	69.7	148.0

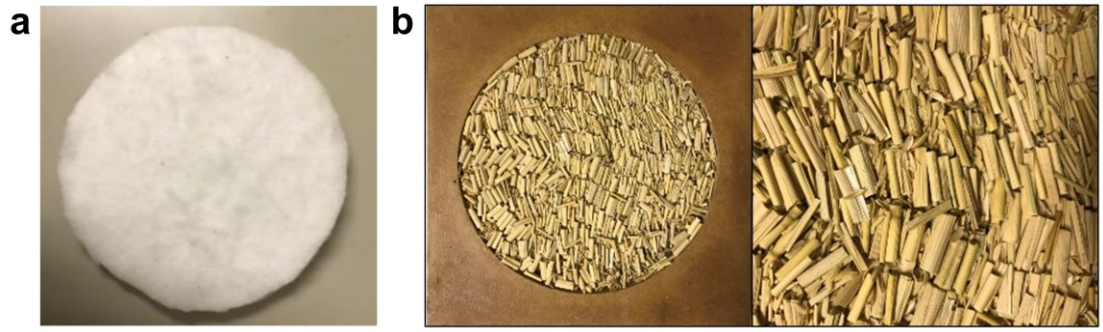

Fig. 4-9. (a) Non-woven (Made by Tokyo-bouon corporation). (b) Absorber mixed with thin rice straw and Rice husks.

Fig. 4-10 (a-c) shows each sample's sound absorption coefficient when the air layer was 0, 15, and 30 mm. The sound absorption coefficient is shown only when the air layer was 30 mm. This indicates that the sample mixed with thick straws and rice husks was very good at absorbing sound in the medium frequency below 900 Hz. However, the bulk density of the sample mixed with thick straws and rice husks was 148.0 kg/m^3.

Since the weight was more than five times that of non-woven fabric, it may not be suitable for places where weight is an issue. A comparison of the samples showed that the sample mixed with thick straws and rice husks showed a higher sound absorption coefficient of about 0.1 on average over the entire frequency range. This is related to the fact that the opportunities for sound waves to enter the acceptable gaps between the rice straws increased and that the rice husks easily entered the gaps between the rice straws, increasing the viscous resistance.

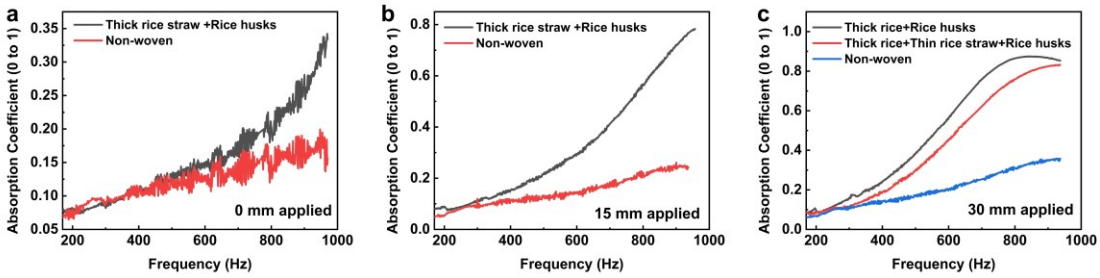

Fig. 4-10. Sound absorption coefficient of Rice straw and Rice husks absorber and Non-woven with different air cavity.

Fig. 4-11 (a-d) show the characteristic impedance, damping constant, and phase velocity of the sample mixed with thick rice straw and rice husks and the nonwoven fabric. Regarding phase velocity, the composite structure of the rice straw and rice husk's attenuation constant value indicates that the absorption of the sound wave translators in the material was significant. The phase velocity showed the smallest value, this means that more resistance is encountered in the propagation of sound, such as stagnation in the solid part of most sound-energy materials, and more vibrations are

generated, lost, and consumed by the interaction in the rice straw and rice husk composite sample. Reflecting that the composite structure's impedance was the largest and thought to be related to the higher sound absorption coefficient than the non-woven fabric.

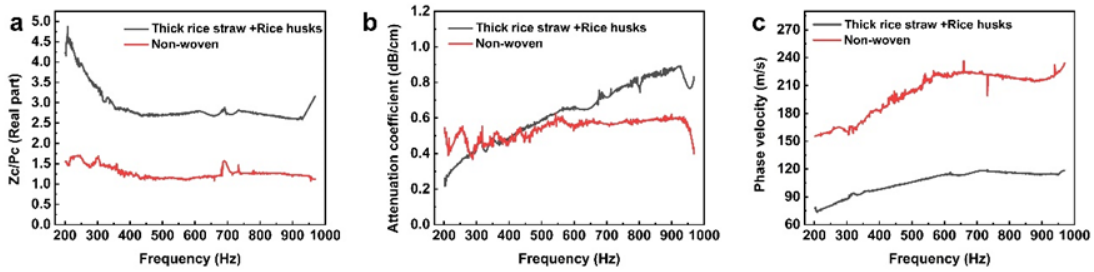

Fig. 4-11. (a) *Zc/pc* of the rice straw and rice husks absorber and non-woven. (Evaluation of absorber mixed with tick rice straws and rice husks). (b) The attenuation coefficient of the rice straw and rice husks absorber and non-woven. (c) The phase velocity of the rice straw and rice husk absorber and non-woven.

4.3.4 Sound absorption properties of composite laminated structure

In this section, we propose a laminated structure in which a porous material is placed behind a perforated plate, as shown in **Figure 4-12**, which is the most effective for sound absorption in the mid-frequency region. A perforated plate (thickness: 4 mm, pore diameter: 6 mm, pitch: 25 mm) and a sample (thickness: 15 mm, volumetric density: 137.4 kg/m³) filled with a mixture of thick rice straws and rice husks were laminated to form a natural material. A multi-layer sound-absorbing structure consisting of a multi-layer sound-absorbing structure was used in which white cuons (thickness:

15 mm, volume density: 27.6 kg/m³) were laminated. Also, there was a 4 mm gap between the MDF perforated plate and each porous material due to the use of the specimen holder.

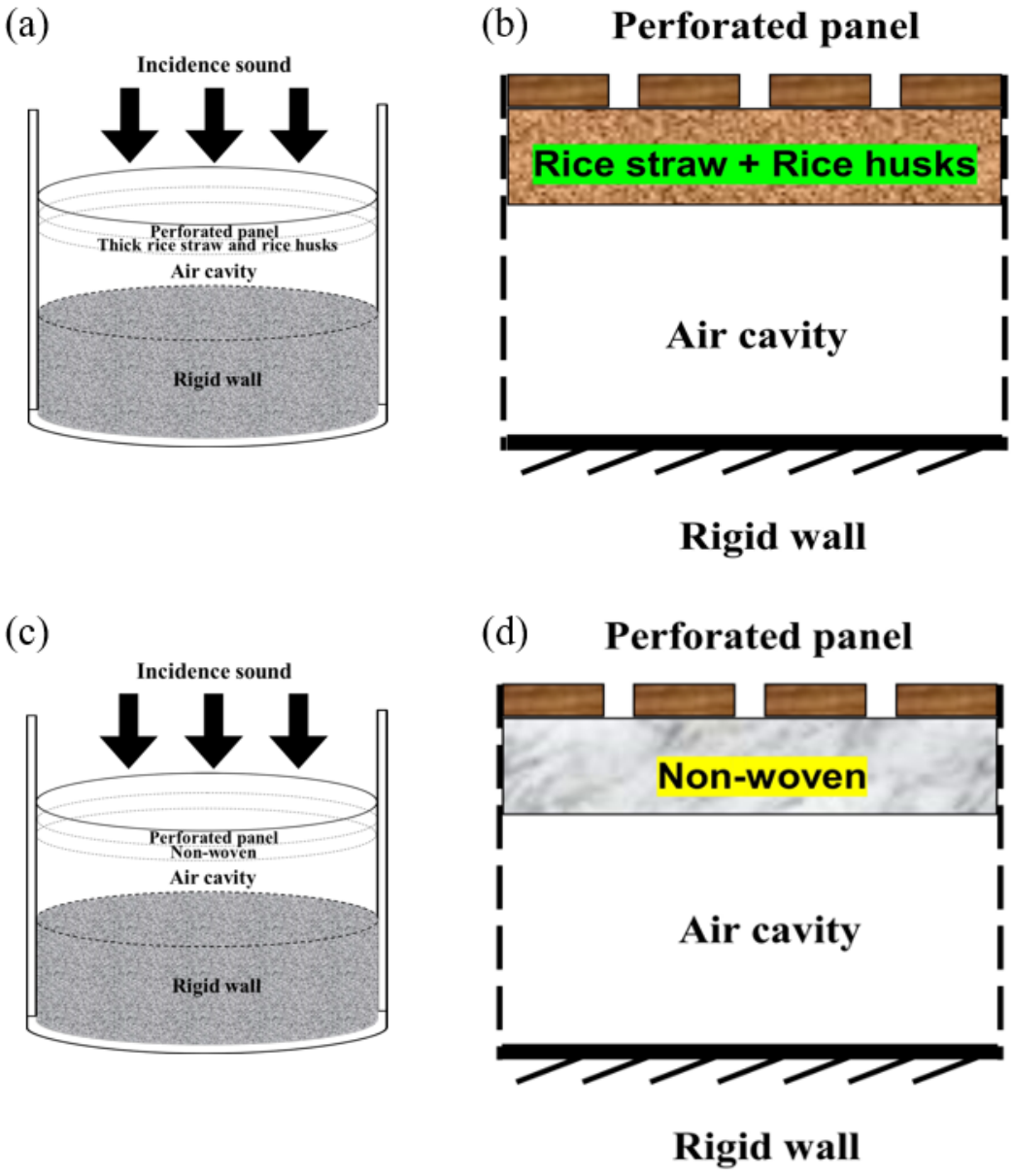

Fig.4-12. 3D section view of the multi-layer (a) perforated panel, thick rice straw and rice husks, (c) perforated panel, non-woven. Multi-layer structure composed of (b) perforated panel, thick rice straw and rice husks, (d)perforated panel, non-woven.

Fig. 4-13 show the measured values of the sound absorption coefficients of the multi-layer sound absorbing structures when the air layer is 15 mm and 30 mm. The frequency of the resonance peak is about 90 Hz lower and the sound absorption coefficient is about 0.06 higher in the structure using the mixed sample. From the above, it was found that the resonance peak due to the vibration of the air appeared on the lower frequency side and the sound absorption coefficient increased in the structure using the sample mixed with thick rice straw and rice husk. Since the peak is considered to be coupled with the resonance peak due to bending vibration of the perforated plate, there is a difference from the original resonance peak frequency, and the sound absorption coefficient is thought to be smaller than this.

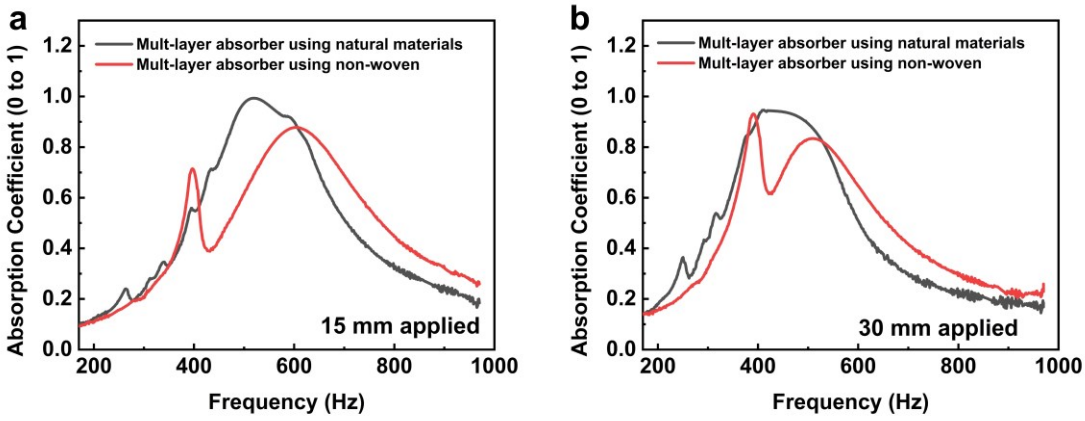

Fig.4-13. Sound absorption coefficient of multi-layer absorber with different air cavity. (Experimental value)

Therefore, in order to eliminate the influence of the bending vibration of the perforated plate and evaluate it, we used the characteristic impedance and propagation constant of each porous material to estimate the sound absorption coefficient of the multi-layer sound absorption structure by the transfer matrix method. **Fig. 4-14 (a and b)** show the predicted values of the sound absorption coefficient of the multi-layer sound absorbing structure when the air layer is 15 mm and 30 mm. The resonance peak frequency was about 90 Hz lower and the sound absorption coefficient was about 0.03 higher in the structure using the sample mixed with rice straw and rice husk. Compared to the measured values, the shift width of the resonance peak frequency was the same, and the rise width of the sound absorption coefficient was smaller. This is thought to be because the sound absorption coefficient of the MDF was high (from section 4.6 of this chapter), and the elasticity of the sound absorption layer behind the perforated plate of MDF was easier to change.

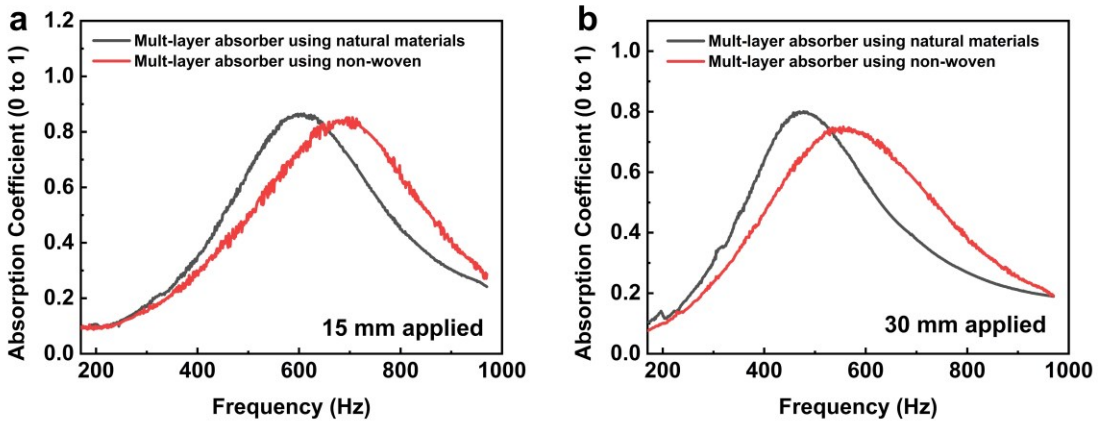

Fig. 4-14. (a) Sound absorption coefficient of multi-layer absorber with different. (Calculated value)

The sound-absorbing elements in porous materials dissipate sound waves through the vibration of the air, which may include viscous damping during sound wave propagation, damping in the air-borne path in the material, vibration damping due to the dynamic elastic behaviour of the porous structure, damping in the solid-borne path, air-solid interaction, and damping due to heat conduction, heat exchange, and other factors. From the above, it was found that using samples of thick rice straws and rice husks as porous materials to construct a multi-layered sound-absorbing structure will lead to superior sound-absorbing performance especially in the low-frequency region. For the multi-layer structure, the sound waves propagating through the samples may cause more air vibrations and consume more acoustic energy. Thus, the sound absorption coefficient of thick rice straw and rice husk samples was superior.

4.4 Conclusion

The sound absorption characteristics were evaluated by classifying the rice straw into thick, thin, and mixed groups, and the optimum thickness was clarified. We constructed a multi-layered sound-absorbing structure using natural sound-absorbing materials and compared its sound-absorption characteristics with a non-woven fabric to evaluate its practicality. The findings are summarized below:

When the thick rice straw was used, it was found that the thick group with a diameter of 3 mm or more had the best sound absorption characteristics. The thick rice straw samples mixed with rice husks showed better sound-absorbing properties than samples

mixed with rice husks, regardless of the thickness, which is much better than non-woven fabrics. It was also revealed that a multi-layered sound-absorbing structure consisting of perforated MDF plates and samples of thick rice straws and rice hulls had better sound absorption performance at the low-frequency side than that of a multi-layered sound-absorbing structure using the non-woven fabric.

Reference

[1] L. Cao, Q. Fu, Y. Si, B. Ding, J. Yu, *Compos Commun*,**10**, 25-35 (2018).

[2] L. Lv, J. Bi, C. Wei, X. Wang, Y. Cui, H. Liu, *Fibers Polym*, **16**, 1562-1567 (2015).

[3] H. Mamtaz, M-H. Fouladi, M. Al-Atabi, S-N. Namasivayam, *J Engin*, **2016**, 1-11 (2016).

[4] J-P. Arenas, M-J. Crocker, *Sound Vibration*, **44**, 12-18 (2010).

[5] M. Liang, H. Wu, J. Liu, Y. Shen, G. Wu, *J Porous Mater*, **29**, 869-892 (2022).

[6] D. Zong, L. Cao, X. Yin, Y. Si, S. Zhang, J. Yu, B. Ding, *Nat Commun*, **12**, 6599 (2021).

[7] M. Toyoda, K. Sakagami, M. Okano, T. Okuzono, E. Toyoda, *Appl Acoust*, **116**, 331-316 (2017).

[8] K. Kalauni, S-J. Pawar, *J Porous Mater*, **26**, 1795-819 (2019).

[9] MA. Shaid Sujon, A. Islam, VK. Nadimpalli, *Polym Test*, **104**, 107388 (2021).

[10] KC. Opiela, TG. Zieliński, *Compos Part B-Eng*, **87**, 107833 (2020).

[11] J. Cucharero, T. Hänninen, T. Lokki, *Acoust*, **2**, 753-765 (2020).

[12] L. Yuvaraj, S. Jeyanthi, *Build Acoust*, **27**, 3-20 (2020).

[13] D. Wang, L. Ying, Y. Jia, L. Zhang, F. Zhang, W. Wang, *J Clean Prod*, **245**, 118911 (2020).

[14] K. Persson, M. Smith, L. Hussain-Alkhateeb, A. Koopman, M. Ögren, E. Peris, W. David, J. Woodcock, C. Sharp, *Environ. Polluti.,* **245**, 558-567 (2019).

[15] H. Ryoo, W. Jeon, *Inter J Mech Sci*, **229**, 107508 (2022)

[16] Q. Liang, Y. Wu, P. Lv, J. He, F. Ma, T. Chen, *Adv. Eng. Mater*, **23**, 2100791 (2021).

[17] F. Martellotta, *Mater*, **14**, 1954 (2021).

[18] PP. Das, V. Chaudhary, F. Ahmad, A. Manral, S. Gupta, P. Gupta, *Polym Compos*, **43**, 1221-1237 (2022).

[19] Z. Liu, J.Z. Yang, S.S. Clark, M.A. Shelly, *Environ Dev Sustain*, **24**, 11011-11026 (2022).

[20] N. Goto, T. Tabata, K. Fujie, T. Usui, *Energy*, **30**, 1259-1270 (2005).

[21] C. Zhang, H. Li, J. Gong, J. Chen, Z. Li, Q. Li, M. Cheng, X. Li, J. Zhang. *Text Res J*, **93**, 1-3 (2022).

[22] NH. Bhingare, S. Prakash, VS. Jatti, *Polym Test*, **80**, 106142 (2019).

[23] Y. Tao, M. Ren, H. Zhang, T. Peijs, *Appl Mater Today*, **24**, 101141 (2021).

[24] L. Chang, A. Jiang, M. Rao, F. Ma, H. Huang, Z. Zhu, Y. Zhang, Y. Wu, B. Li, Y. Hu, *RSC Adv*, **11**, 37784-37800 (2021).

[25] DJ. Oldham, CA. Egan, RD. Cookson, *Appl Acoust*, **72**, 350-363 (2011).

[26] S. Mehrzad, E. Taban, P. Soltani, SE. Samaei, A. Khavanin, *Build Environ*, **211**, 108753 (2022).

[27] F. Asdruball, S. Schiavoni, K.V. Horoshenkov, *Build Acoust*, **19**, 283-312 (2012).

[28] C. Rubino, M.B. Aracil, J.G. Payá, S. Liuzzi, P. Stefanizzi, M.Z. Cantó, F. Martellotta, *Mater*, **12**, 4020 (2019).

[29] C. He, J. Huang, S. Li, K. Meng, L. Zhang, Z. Chen, Y. Lai, *ACS Sustain Chem. Eng*, **6**, 927-936 (2017).

[30] Y. Chen, F. Yuan, Q. Su, C. Yu, K. Zhang, P. Luo, D. Hu, Y. Guo, *J Clean Prod*, **245**, 118917 (2020).

[31] Z.Y. Lim, A. Putra, MJM Nor, M.Y. Yaakob, *Appl Acoust*, **130**, 107-114 (2018).

[32] K. Tsukui, R. Saito, T. Yamaguchi, *ICTSS*, 1-9 (2020)

[33] H.S. Kim, P.S. Ma, S.R. Kim, S.H. Lee, Y.H. Seo, *J Sound Vib*, **430**, 75-92 (2018).

[34] Standard ISO 10534-1, Acoustics－ Determination of sound absorption coefficient and impedance in impedance tubes Part 1 (1998).

[35] Standard ISO 10534-2, Acoustics－Determination of sound absorption coefficient and impedance in impedance tubes Part 2 (1998).

[36] W.D. Yang, H. Xia, T. Natsuki, Q-Q. Ni, *Fiber Sci. Technol*., 79(4), 72-81 (2023).

[37] Standard ASTM E1050-98. Standard test method for impedance and absorption of acoustical materials using a tube, two microphones and a digital frequency analysis system;1998.

[38] Kinsler LE, Frey AR, Coppens AB, Sanders JV. Fundamentals of acoustics 4th ed. Wiley-VCH; 1999.

[39] Allard J, Atalla N. Propagation of sound in porous media: modelling sound absorbing materials. 2nd ed. John Wiley and Sons; 2009.

Chapter 5: General conclusion

In this work, we developed a new sound absorbing device with excellent sound absorption performance for noise problems. The sound absorption effect of the developed structure and the mechanism of sound wave propagation is investigated. In addition, a laminated sound-absorbing structure using natural straw and rice husk was designed. The obtained main results are as follows:

In chapter 1, an overview of sound absorption materials and structures are discussed.

In chapter 2, we proposed a single cavity resonant device (SCRD) and a new double cavity resonant device (DCRD) with multi-band sound absorption characteristics. Two air cavities with a sound-absorbing material in the neck of the DCRD and a microperforated board inside the Helmholtz resonator are designed. The absorption coefficients and peak frequencies are systematically discussed. The findings revealed that the DCRD's sound absorption performance is more than two times higher than that of the Helmholtz resonance structure. The developed DCRD could almost absorb low-frequency sounds without sacrificing high-frequency performance by using the microperforated board of MPP 3. The optimization of absorption behavior is obtained, especially in the low-frequency region, which may offer a flexible design approach without increasing the structure's size. In addition, it is clarified that the absorption effect of SCRD with wave foam is better than that of flat foam, and the continuous round hole shape is better than slit holes.

In chapter 3, the sound absorbing characteristics of the DCRD with the insertion of various sound-absorbing porous materials combining MPPs are investigated. The results reveal that the sound absorption performance of DCRD is more than twice that

of the Helmholtz resonance structure. And the developed DCRD could almost absorb low-frequency sounds without sacrificing high-frequency performance with the insertion of MPPs.

In chapter 4, a laminated sound-absorbing structure using natural straw and rice husk is designed. By classifying the rice straw into different groups, their sound absorption characteristics were evaluated and optimized. It was found that a multi-layered sound absorbing structure consisting of perforated MDF plates and samples of thick rice straw and rice hulls has better sound absorption performance on the low frequency side than a multi-layered sound absorbing structure using non-woven fabric.

In chapter 5, a summary of this work and conclusions were presented.

In summary, we believe this work provides a new toolbox for enriching the family of resonant sound absorption materials, especially realizing noise reduction optimization of low-frequency sounds through a flexible design approach without increasing the structure size.

Published papers

The dissertation based on following published papers:

・**Wendan Yang**, Hong Xia, Qing-Qing Ni. A double cavity resonant device embedded with porous material and microperforated panel. Appl. Acoust., 206, 109304 (2023).

・**Wendan Yang**, Hong Xia, Toshiaki Natsuki, Qing-Qing Ni. Design and fabrication of double cavity resonant structure towards low-frequency sound absorption improvement. J. Fiber Sci. Technol., 79(4), 72-81 (2023).

・**Wendan Yang**, Hong Xia, Toshiaki Natsuki, Qing-Qing Ni. Design and properties of the laminated sound-absorbing materials using natural straw and rice husk. J. Fiber Sci. Technol., 79(4), 92-100 (2023).

Acknowledgments

Firstly, I sincerely thank my supervisors, Prof. Toshiaki Natsuki and Prof. Qing-Qing Ni, for the guidance and valuable discussion throughout my PhD research.

I would also like to thank all the staff members from Shinshu University who provided me with experimental and technical support.

Special thanks to my academic colleagues and friends. Hao Wang, Toyohara, Ikeda, from the Natsuki LAB and Ni LAB in Shinshu University during my PhD research.

I also give my thanks to the scholarship received from Shinshu University supporting my academic (2019，2020) from the Japan Student Service Organization (JASSO).

Finally, I would like to express my great thanks to my family. Thank you for my husband's hard work and effort in our family. And thank you for your support and encouragement during my PhD research.